KfK 3189
November 1981

# Transition from Slug to Annular Flow in Horizontal Air-Water and Steam-Water Flow

J. Reimann, H. John, W. Seeger
Institut für Reaktorbauelemente
Projekt Nukleare Sicherheit

Kernforschungszentrum Karlsruhe

KERNFORSCHUNGSZENTRUM KARLSRUHE

Institut für Reaktorbauelemente
Projekt Nukleare Sicherheit

KfK 3189

# TRANSITION FROM SLUG TO ANNULAR FLOW IN HORIZONTAL AIR-WATER AND STEAM-WATER FLOW

J. Reimann, H. John, W. Seeger

Kernforschungszentrum Karlsruhe GmbH, Karlsruhe

Kernforschungszentrum Karlsruhe GmbH
ISSN 0303-4003

## Übergang von der Schwall- zur Ringströmung in horizontaler Luft-Wasser- sowie Dampf-Wasser-Strömung


### Zusammenfassung

Es wurde der Übergang von der Schwall- zur Ringströmung in horizontaler Luft-Wasser- sowie Dampf-Wasser-Strömung untersucht. Teststrecken mit 50, 66,6 und 80 mm Innendurchmesser wurden verwendet. Der Systemdruck betrug 0,2 und 0,5 MPa bei den Luft-Wasser-Experimenten und 2,5; 5; 7,5 und 10 MPa bei den Dampf-Wasser-Experimenten. Zur Bestimmung der Strömungsform wurden lokale Impedanzsonden verwendet. Diese Methode wurde in einem Teil der Versuche mit Differenzdruck- und Gamma-Strahl-Messungen verglichen.

Die Grenze zwischen den beiden Strömungsformen verschiebt sich mit zunehmendem Druck wesentlich zu kleineren Werten der Gasvolumen-Stromdichte (superficial gas velocity). Aus der Literatur bekannte Korrelationen stimmen nur unbefriedigend mit den Experimenten überein. Eine neue Korrelation wird vorgeschlagen.


## Transition from Slug to Annular Flow in Horizontal Air-Water- and Steam-Water-Flow


### Abstract

The transition from slug to annular flow in horizontal air-water and steam-water flow was investigated. Test sections of 50; 66.6 and 80 mm ID were used. The system pressure was 0.2 and 0.5 MPa in the air-water experiments and 2.5; 5; 7.5 and 10 MPa in the steam-water experiments. For flow pattern detection local impedance probes were used. This method was compared in a part of the experiments with differential pressure and gamma-beam measurements.

The flow regime boundary is shifting strongly to smaller values of the superficial gas velocity with increasing pressure. Correlations from literature fit unsatisfactorily the experimental results. A new correlation is presented.

CONTENTS page

## 1. INTRODUCTION

The prediction of the flow pattern of a gas-liquid mixture in a pipe is very important for many technical applications because pressure drop, heat and mass transfer are strongly dependent on the flow pattern. The knowledge of flow patterns was also important in the tests and calibrations of various two-phase mass flow rate instrumentations /1/ because the signals of some instruments were strongly affected by the flow pattern. The experimental data presented in this paper originate to a great part from these test series performed in the last years. Some results were already presented previously /2/; this report contains additionally a more detailed description of the flow pattern transition mechanisms and more examples of phase distribution measurements of different flow patterns.

For flow pattern prediction either flow regime maps are used, based on experimental data or models are used based on physical mechanisms for the existence of certain flow patterns. Beginning with the early flow maps, e. g. from Baker /3/ there has been a continuous discussion on the choose of appropriate coordinates. Whereas in the beginning one attempted to describe all flow regime boundaries with a single pair of coordinates, in more recently published articles (see e. g. /4-7/) each single boundary is expressed in different terms of dimensionless goups containing the flow parameters, the fluid properties and the pipe diameter. Most often a map with the superficial velocities of the liquid phase $V_{sl}$ and the superficial velocity of the gas phase $V_{sg}$ as coordinates is used and the influence of the other parameters is demonstrated in such a map.

Figure 1, on the left hand side, shows the flow map developed by Mandhane /4/ for air-water flow near atmospheric pressure. On the right hand side correlations from other authors /3-9/ are shown for the boundary between the slug flow (intermittend flow) and annular droplet flow again for the air-water system at atmospheric pressure and a pipe diameter of 50 mm. It is demonstrated that the differences between the different correlations can become considerable already for this comparatively well known fluid system.

The fluid system steam-water is of special importance for technical applications and thus the importance for predicting the flow pattern. However, experimental data for this system are comparatively rare and mainly restricted on small pipe diameters ($d \lesssim 25$ mm) and vertical flow direction. The changes of the fluid properties of this fluid system can become very large compared to the system air-water and therefore this system is a good check for the various correlations of flow pattern predictions.

In this article the air-water and steam-water data are presented in a map with the superficial velocities as coordinates and it is tried to elaborate the influence of the dominating parameters on the boundary between slug and annular droplet flow.

## 2. CHARACTERISTICS OF SLUG AND ANNULAR FLOW IN HORIZONTAL PIPES

Certain variations of flow patterns already exist within a flow regime because each flow regime covers a certain range of parameters. The boundaries between flow regime are not sharp lines but the transition from one flow regime to the other again covers a certain range of parameters. Therefore already the descriptions for socalled well developed flow patterns are differing. Concerning the transition between flow regimes the variations of opinious are even larger.

Slug flow is the most important intermittend flow pattern: slugs which fill the total pipe cross section propagate through the pipe followed by a phase distribution consisting of gas in the upper portion and liquid in the lower portion of the pipe. The higher the volumetric gas flow, the higher is the void fraction in the slugs; the entrainment of bubbles in the liquid layer also increases. If the gas phase becomes the continuous phase in the slug some workers take this as characteristic for the transition from slug to annular flow (compare e.g. /9/) whereas other workers (e.g. /10/) still asign this flow pattern (surge flow) to the slug flow regime.

Annular flow in horizontal pipes is characterized by a thick liquid layer at the bottom of the pipe with a certain entrainment of bubbles and a thin liquid layer at the upper part of the pipe. The transport of liquid from the lower to the upper portion of the pipe is caused by disturbance waves or the entrainment-deposition process though other mechanisms may also exist (compare e.g. /11/). The latter mechanism is mostly used in literature to characterize annular flow: droplets are torn off mainly from the lower interface and are entrained in the gas flow. The droplets which are deposited at the upper pipe wall give rise to a thin liquid film which flows downward due to gravity.

For the transition from slug to annular flow, the following description was given in /9/: "As the gas rate and consequently the slug velocity increase, the degree of aeration of the slug increases. Ultimately the gas forms a continuous phase through the slug. When this occurs the slug begins bypassing some of the gas. At this point the slug no longer maintains a competent bridge to block the gas flow so the character of the flow changes. This point is the beginning of 'blow-through' and the start of the annular flow regime."

In /12/ the transition is also characterized by the bypassing effect of the gas: "As the gas velocity increases still further the slug become pierced with a gas core and the flow becomes essentially annular".

An excellent photography from a slug flow near the transition to annular flow is shown in /13/: The slug consists of a foamy mixture, between the slugs a highly aerated layer flows with a rough interface and rupture of liquid filaments occurs.

At low volumetric liquid flow rate, near the transition region from slug to wave flow, large instable waves sweeping through the pipe, intermittently wetting the upper wall were observed by /14/ and /15/ at a parameter range which other workers (e.g. /16/, /17/) still asigned to the slug flow regime. Again, because of lack of appropriate measuring technique, it is difficult to decide if these disturbances fill the total pipe cross section and then are similar to the surges described by /10/ or are similar to the disturbances waves described by /11/ which can occur even in so-called well developed annular flow. A criteria to differentiate between these two mechanisms perhaps could be based on the frequencies of these "disturbances". It is known (compare e.g. /18/) that the slug frequencies increase with increasing liquid fraction and to a smaller extent with the total volume flow rate. If the liquid flow rate is kept constant and the gas flow rate is increased the slug frequency does not change considerably. On the other hand it is expected that the disturbance wave frequencies generally are different from the slug frequencies because the mechanism to generate these disturbances is different. This should be true also in the neighbourhood of the flow regime transition. This phenomena will be looked at in detail later.

The knowledge on the transition from slug to annular flow at horizontal steam-water flow at high pressures is very small. In /19/ it was shown that a flow pattern without slugs exists at a system pressure of 10 MPa and quite low volumetric flow rates, characterized by a approximately constant gradient of the vertical void fraction profile. This flow pattern was designated as stratified dispersed flow because in the lower part bubbles are entrained in the liquid phase; in the upper part droplets are entrained in the gas phase. A defined interface level could not be measured. This implies that the mechanism at the very rough interface (liquid rupture and

bubble entrainment) is the dominating process. The tendency of waves to grow and finally bridge the pipe is probably strongly damped out.

Experiments with acetate and water, a fluid system with a phase density ratio even smaller than at steam-water at 10 MPa were presented in /20/: the flow pattern can be very similar to the above mentioned stratified dispersed flow pattern.

In the following a difference is only made between slug flow (intermittend flow) and annular flow (more precisely: annular droplet flow). A flow pattern is attributed to the slug flow regime if intermittend gas-liquid slugs exist, filling the total pipe cross section. A flow pattern is attributed to the annular droplet regime if droplets exist near the upper pipe wall giving rise to a liquid film. With these definitions the stratified dispersed flow pattern is attributed to the annular droplet flow regime.

## 3. FLOW PATTERN DETERMINATION

A overview on the large number of publications concerning various measuring techniques of flow patterns is given in /21/. In our experiments a local impedance probe was used; this technique and some results had been presented already in previous papers /19/ and /22-25/. Figure 2 shows schematically the probe and probe signals if the probe tip is surrounded by dispersed bubble flow (upper part) or dispersed droplet flow (lower part). In horizontal flow the phase distribution can vary considerably in the cross section. Figure 3 shows for an annular flow pattern signals at different locations along the vertical diameter, obtained with a traversable probe. It is seen that a dispersed bubble mixture exists near the bottom of the pipe and a dispersed droplet flow in the upper part of the pipe. Figure 4 shows probe signals for a slug flow: in the upper part of the pipe, a dispersed bubble flow type signal alterates with a signal at the gas level. In the lower part of the pipe the mixture becomes more homogeneously mixed. As indicated in Figure 2 the time averaged local void

fraction can be measured using a suitable trigger level. Figures 3 and 4 contain some vertical void fraction profiles, Figure 4 additionally some horizontal profiles.

Taking probe signals at many positions is very tedious but the benefit is a quite detailed picture of the flow pattern. If the only purpose is to differ between intermittend and annular flow, it is not necessary to take as many measurements. It proved to be sufficient to measure at a distance of about 15 % of the diameter below the upper wall. (However, in our experiments always more measurements were made). To determine quantitatively the flow regime boundary, the power spectral density function is very suitable as demonstrated later.

As mentioned previously in most of the experiments other two-phase flow instrumentations such as drag disks, turbine meters, gamma densitometers, differential pressure transducers etc were available in the test-section. It is easy to demonstrate that other instruments are also able to determine flow patterns in certain conditions (comparisons of impedance probe signals with three beam LOFT type densitometer signals are presented in /25/), but the other techniques proved to be less sensitive if the transition between flow regimes was looked for. Further examples for the use of other instruments are presented later.

## 4. TEST FACILITY

The test facility which is described in detail in /26/ consists of a steam-water and an air-water loop. To enable a proper comparison between the two fluid systems both loops use the same mixing chamber and horizontal test section. Figure 5 shows schematically the steam-water loop which can be operated at pressures up to 15 MPa, mass flow rates up to 5 kg/s and qualities between 0 and 1. Two boilers provide the loop with slightly subcooled water and slightly superheated steam. The single phase mass flow rates are measured with orifices. Then the flows pass sinter metal filters and are combined in the mixing chamber. The horizontal test section with a length of

10 m is followed by a pipe with an inner diameter of 100 mm and a length of 9 m ending with the electrically actuated pressurizer valve controlling automatically the test section pressure. The two-phase mixture is then condensed, the condensate is pumped back and thus the cycle is completed.

The air-water loop has a maximal capacity of 35 kg/s water flow rate and 1 kg/s air flow rate; the maximal pressure is 1,2 MPa. The single phase mass flow rates again are measured with orifices. The test section is followed by a pipe with inner diameter of 100 mm and a length of about 8 m leading the mixture to an air-water separator. About 4 m downstream of test section a valve is positioned to controll the test section pressure. The air is released to the atmosphere and water is pumped back.

Because the phase distribution at the test section inlet is dependent on the way of mixing the phases, the mixing chamber is described more detailed. Figure 6 shows a sectional view: The main component is an expanding thin walled tube provided with about 800 bores of 2 mm diameter. There are two tubes available: one with an inner diameter of 80 mm, the other with an inner diameter of 50 mm. The number of bores can be reduced by using sheet collars to optimize the pressure drop for the stable mode of operation. There are two modes of operation: either the liquid flows through the centrical tube and the gas is dispersed into the liquid through the bores, or if the mixing chamber is rotated by $180^{o}$ the phases are mixed in the reverse way. For both modes of operation the phases at the test section inlet were strongly stratified at low volume fluxes (corresponding to the transition from the wave to the slug flow regime). At high volume fluxes (transition from the slug to the annular flow regime) from visual observations with a lucite test section the phases seemed to be quite homogeneously mixed. However, it is supposed that in the pipe significant differences existed: if gas enters the tube through the bores the phases are probably much more intensively mixed than in the other mode of operation. For the first mode, the water tends to stay concentrated near the pipe wall favoring an annular flow. In connection with this a continuous

gas core reaching from the single phase orifice down to the end of the two-phase test section may occur which enables that small pressure fluctuations at the test section end cause gas mass flow rate fluctuations. If the gas was dispersed into the liquid flow the loop behavior was much more stable and the thermodynamic equilibrium at steam water flow is much faster obtained. Therefore in general the latter way of mounting the mixing chamber was used.

As described previously, the system pressure is controlled by throttling before separating or condensing the two-phase mixture downstream of the test section. This way in general causes larger pressure fluctuations at the test section end than using a gas-liquid separator immediately at the test section end. To minimize these pressure fluctuations throttling could be performed by a valve at the end of the test section and the second valve previously mentioned. The pressure fluctuations are greatest at low volume fluxes (stratified wave flow) and become small in the transition region from slug to annular flow. It is therefore assumed that the special set up downstream of the test section has no significant influence on the results presented in the following.

The tests were performed in air-water and steam-water flow, with test section diameters of 0.05, 0.066, and 0.08 m, Table I contains further details.

## 5. EXPERIMENTAL RESULTS: FLOW PATTERNS

For flow pattern determination in a part of the experiments three different measuring methods were simultaneously used: the traversable impedance probe (IP), a 5 beam gamma densitometer (GD) (described in detail in /27/) and a $\Delta p$-transmitter. Figure 7 shows the experimental set up: The signal of a gamma beam was taken together with the IP-signal at that vertical position which corresponds to the vertical height of the middle of the gamma beam sekant (e.g. signals of beam I and IP at $y/d = 0,92$ were taken simultaneously, etc.). For all combinations $\Delta p$ was also measured.

| Pipe Diameter d (m) | Fluid System | Pressure p (MPa) | Axial Probe Location L (m) | L/d (1) | Nr. of Exp. | Typ of Instrumentation Comments |
|---|---|---|---|---|---|---|
| 0,05 | Air-Water | 0,5 | 8 | 160 | 85 | Traversable Impedance Probe (IP) Partly: Horizontal 5 Beam Gamma Densitometer, Drag Body, Differential Pressure, Transducer |
| | Steam-Water | 2,5 | 8 | 160 | 53 | |
| | | 5,0 | | | 37 | |
| | | 7,5 | | | 23 | |
| | | 10,0 | | | 26 | |
| 0,066 | | 4,0 | 4.4 | 67 | 40 | Two Fixed IP, 10 mm above Bottom and below Top of Pipe, 3 Beam LOFT Densitometer, Drag Disk, Turbine Transducer, 80 mm Mixing Chamber Inlet, Reduction on d = 0,066 m 1.3 m Downstream |
| | | 7,5 | | | 16 | |
| 0,08 | Air-Water | 0,2 | 8 | 100 | 62 | Two Fixed IP, 11 mm above Bottom and below Top of Pipe, Variation of Mixing Chamber Installation |
| | | 0,5 | | | | |

Table I Test Section Geometry and Instrumentation

The Figures 8 - 10 contain steam-water results at 2.5 and 5 MPa from the slug flow regime: in the right part the signals are shown, the left part contains the corresponding power spectral density function (PSDF). The void fraction changes drastically with the vertical distance y/d. However, as long as a significant gas content exists the PSDF shows the typical slug frequency. This is not the case in the lower portion of the cross section in Figure 9 where a pure liquid flows occurs.

Figure 11 shows results for a wave flow pattern at steam-water flow at 10 MPa:

The wavy interface covers only a small range of the vertical distance, below and above the fluid becomes pure single phase liquid and steam, respectively. In these cases the PSDF becomes a straight horizontal line.

Figure 12 contains results for an annular flow pattern at 2.5 MPa. There occurs no distinguished frequency with a high amplitude at any distance. The PSDF for the gamma beams is a horizontal straight line whereas the IP signal covers a broad frequency range. Due to the small amplification of the PSDF signal (constant for all distances) this broad frequency range cannot be seen for y/d = 0,5 and y/d = 0,70. At y/d = 0,92 the amplitudes become larger again; here the probe is in the vicinity of the upper liquid film and rupture of liquid from this film may change the probe signal.

An example for probe signals and PSDFs in a dispersed bubble flow (with $V_{sl}$ = 4 m/s and $V_{sg}$ = 5 m/s) is shown in Figure 13. For these measurements two probes, one near the top (y/d = 0,86) and other near the bottom (y/d = 0,14) of the pipe were used. The phase distribution is quite homogeneous both in time and space. The PSDF covers a broad frequency spectrum but there exist no distinctive frequency peak.

In Figure 13 the superficial gas velocity is kept constant ($V_{sg}$ = 5 m/s) and the superficial liquid velocity is increased from 0,2 to 4 m/s. This corresponds to a traverse from the wave to the dispersed bubble flow regime.

At wave flow ($V_{sl}$ = 0,2 m/s) the PSD again is a horizontal line for the upper probe. The PSD for the lower probe can be similar or contain some frequencies depending on the interface height and wave amplitude.

For the slug flow pattern at low values of $V_{sl}$ it is characteristical that the PSD functions have peaks at different frequencies because not all slugs reach the lower probe. At intermediate values of $V_{sl}$ both frequencies coincide. At high values of $V_{sl}$ a fairly

homogeneous bubble flow exists near the pipe bottom and again the intermitted flow behavior is limited to the upper portion of the cross section.

In Figure 14 the superficial liquid velocity is kept constant ($V_{sl}$ = 1 m/s) and the superficial gas velocity is varied from $V_{sg}$ = 3 m/s to $V_{sg}$ = 28 m/s. This corresponds to a traverse from slug to annular flow regime. In Figure 13 a continuous increase of the slug frequency could be observed with increasing $V_{sl}$. In Figure 14 it is seen for the upper probe that with increasing $V_{sg}$ a second lower frequency peak develops which becomes the dominating frequency near the transition to annular flow. One explanation for this behavior is that due to the decreasing liquid fraction with increasing $V_{sg}$ not all waves can get enough liquid to grow to such a size that they bridge the total pipe cross section.

The upper PSDF indicates clearly that at $V_{sg}$ = 13,5 m/s an annular flow regime exists; the flow regime boundary therefore must be between $V_{sg}$ = 10 and $V_{sg}$ = 13,5 m/s.

Figure 15 shows a similar traverse like Figure 14 but for a high value of $V_{sl}$ where the flow pattern is near the transition to dispersed bubble flow. Up to $V_{sg}$ = 10 m/s the flow pattern belongs to the slug flow regime, the signals at $V_{sg}$ = 15 m/s are characteristical for the transition between slug, annular and dispersed bubble flow.

## 6. EXPERIMENTAL RESULTS: FLOW REGIME BOUNDARIES

The Figures 16-23 show the detected flow regimes. Between Figure 16 and 17 the pipe diameter was changed form 50 to 80 mm. For the 50 mm ID pipe experiments it is more difficult to determine the boundary than for the 80 mm ID pipe experiments because the number of test points in the interesting range is considerably lower. The boundary for the 50 mm pipe seems to be shifted to slightly higher values of $V_{sg}$. This effect is opposed to the

expected tendency and may be not a real diameter effect but an influence of the different L/d ratio. However this effect is small; no clear difference also was found in steam-water flow experiments with the 50 and 66.6 mm ID test section. Therefore it is concluded that for the diameter range investigated there is no significant diameter effect.

The Figures 17 and 18 contain air-water flow results at two different gas densities (system pressures). With increasing pressure (increasing gas density) the boundary is shifted to lower values of $V_{sg}$. The dependency of the boundary is about proportional to $(\rho_g)^{-0,4}$.

The Figures 17 and 19 show results for different modes of mixing chamber installation. For the experiments in Figure 19 the water was dispersed into the centrical gas flow. Annular flow is therefore reached at lower values of $V_{sg}$ at high values of $V_{sl}$ as already mentioned earlier.

The Figures 20 to 23 contain steam-water data for different pressures and the test section diameter d = 0,05 m. The Figures 22 and 23 contain additionally data with d = 0,066 m at p = 4 MPa and p = 7.5 MPa, respectively. Only a few of these test points are near the transition region from slug to annular flow. For further discussions it is therefore assumed that the flow regime boundaries plottet in the Figures 22 and 23 are representative for d = 0,05 m and a pressure of 4 and 7.5 MPa, respectively.

The Figure 24 contains a comparison of our air-water results at the lowest system pressure investigated (p = 0,2 MPa) and the pipe diameter d = 0,08 m with air-water experiments near atmospheric pressure published recently /14, 18/ and values calculated from various correlations /3-8/ for our test conditions. Similar to Figure 1, Figure 24 again shows the discrepancy between the results taken from literature. Our experimental results group fairly well in the middle of the various other results, a good agreement is obtained with the recently

published data /28/; the two curves 2a and 2b belong to different mixing chamber positions.

Figure 25 contains experimental results for the 0,05 m ID test section for air-water flow at 0,5 MPa and steam-water flow at 2,5 - 10 MPa. These results again are compared with different empirical correlations (left hand side) and correlations based on a more mechanistic approach(right hand side). To get an impression on the influence of the single parameters these correlations are briefly listed:

Baker flow map /3/: This flow map does not contain the pipe diameter as a parameter. The boundary abscissa and ordinate depend on the following expressions

$$\frac{V_{sg}}{V_{sg_o}} = \left(\frac{\rho_l}{\rho_{l_o}} \cdot \frac{\rho_{go}}{\rho_g}\right)^{0.5} \tag{1}$$

and

$$\frac{V_{sl}}{V_{sl_o}} = \frac{V_{sg}}{V_{sg_o}} \left(\frac{\rho_g}{\rho_{g_o}}\right)^{0.5} \frac{\sigma}{\sigma_o} \left(\frac{\rho_{lo}}{\rho_l}\right)^{0.17} \left(\frac{\mu_{lo}}{\mu_l}\right)^{0.33} \tag{2}$$

where $\sigma$ is the surface tension und $\mu$ the dynamic viscosity. The index "o" means that the air-water properties at atmospheric pressure and 20 $^{o}$C were used (standard conditions).

Mandhane et al. flow map /4/: Here the boundary shifts only in direction of the abscissa according

$$\frac{V_{sg}}{V_{sg_o}} = \left(\frac{\rho_{go}}{\rho_g}\right)^{0.2} \left(\frac{\rho_{lo}}{\rho_l} \frac{\sigma}{\sigma_o}\right)^{0.25} \left(\frac{\mu_{go}}{\mu_g}\right)^{0.2} \tag{3}$$

Weisman et al flow map /7/: Here the boundary also shifts only in direction of the abscissa in the following way

$$\frac{V_{sg}}{V_{sg_o}} = \left(\frac{\rho_{go}}{\rho_g}\right)^{0.23} \left(\frac{\rho_l-\rho_g}{\rho_{l_o}-\rho_{g_o}}\right)^{0.11} \left(\frac{\sigma}{\sigma_o}\right)^{0.11} \left(\frac{d}{d_o}\right)^{0.415} \quad (4)$$

with $d_o$ = 0,0254 m.

Wallis correlation /8/: The transition takes place at a constant value of $V_{sg}$ for a certain fluid system and pressure:

$$V_{sg} = 0,9\ (gd)^{0.5} \left(\frac{\rho_l-\rho_g}{\rho_g}\right)^{0.5} \quad (5)$$

Taitel-Dukler correlation /5/: These authors give the following expression

$$V_{sg} = 0,593\ \left(\frac{\rho_l}{\rho_g}\right)^{0.444} \left(\frac{\mu_l}{\mu_g}\right)^{0.111} V_{sl} \quad (6)$$

Simpson et al correlation /6/: These authors developed the relationship given below

$$V_{sg} = 16,5\ \frac{g^{0,145}\ \sigma^{1,163}\ d^{0,821}\ \cdot\ \rho_l^{0,013}}{\rho_g^{0,5}\ \mu_l^{0,676}}\ \frac{1}{V_{sl}^{0,941}} \quad (7)$$

Figure 25 demonstrates impressively the large deviations between these correlations: There is no correlation which fits all experiments satisfactorily.

The following comments are briefly made

- the steam-water results show a large shift of the boundary ($V_{sg\ 2.5\ MPa}/V_{sg\ 10\ MPa} \approx 4,4$ at $V_{sl}$ = 1 m/s). A similar behavior is only described with eq. (7)
- the dependence of the boundary on $V_{sl}$ is comparatively weak. This corresponds to the correlation given by eq. (5)
- Comparing the air-water and steam-water results it is seen that the shift is not as large as it could be expected from the density change. Changing from air-water to steam-water flow the liquid viscosity $\mu_l$ changes considerably. This effect may

compensate somewhat the density and surface tension effect. The only correlation which describes this tendency is given by eq. (5). However this equation seems to overpredict this effect.

- From the six correlations used for comparison three correlations (eq. (1), (3), (6)) do not contain any influence of the pipe diameter, whereas the other correlations (equations (4), (5), (7)) contain a relatively strong pipe diameter influence. The present experiments indicate that if there is an diameter influence, the influence is quite small.

Besides the correlations presently discussed there exist various other empirical correlations; e.g. Mayinger and Zetzmann /29/ proposed a generalized flow regime map for one component fluid systems and vertical upward flow where the property changes were taken into account by the function $(p/p_{crit})^{-n}$. No value was found for the exponent n which yielded an improved fit of the steam-water results.

Taking into account the previous discussions the following correlation is proposed:

$$V_{sg} = 0,285\,(g\cdot d)^{1/6} \quad \frac{\sigma^{2/3}}{(\mu_l \mu_g)^{1/3}} \quad \left(\frac{\rho_l - \rho_g}{\rho_g}\right)^{0,4} \tag{8}$$

Table II shows a comparison between measured values of $V_{sg}$ for the boundary and corresponding values from eq (8) for a superficial liquid velocity $V_{sl}$ = 1 m/s.

Eq.(8) is independent on $V_{sl}$; in a flow map with $V_{sl}$ and $V_{sg}$ as coordinates eq.(8) therefore gives a vertical line. For $V_{sl} > 1$ m/s and $V_{sl} < 1$ m/s eq.(8) predicts in general values which are too low and too high, respectively. However, the agreement compared to other correlations is very satisfactory.

| d(m) | p(MPa) | fluid system | $V_{sg}$ boundary (m/s) measured | from eq. (8) |
|---|---|---|---|---|
| 0,05 | 0,5 | air-water | 13,0 | 12,8 |
| | 2,5 | steam-water | 11,0 | 11 |
| | 5 | steam-water | 7,7 | 6,7 |
| | 7,5 | steam-water | 4,0 | 4,4 |
| | 10 | steam-water | 2,9 | 2,6 |
| 0,08 | 0,2 | air-water | 16,5 | 20,0 |
| | 0,5 | air-water | 12,0 | 13,9 |

Table II Measured and Calculated Flow Regime Boundary Values

## 7. CONCLUSIONS

There is a great need for reliable flow pattern correlations especially for steam-water flow. To develop and check such correlations corresponding experiments have to be performed.

It has been demonstrated that the local impedance probe is a very sensitive instrument for flow regime detection. With a traversable probe many details of the flow pattern can be obtained, e.g. void profiles /19/, bubble distribution etc. In present and further experiments this probe is combined with a small pitot tube /30/, /31/ which even gives an impression on the local velocity and mass flow rate distribution.

The correlations for the transition between slug and annular flow developed by other authors do not fit satisfactorily our experimental results. A new correlation was proposed which has to be checked with experiments from other authors.

In this paper only the slug to annular flow transition was discussed. Together with additional data the boundaries between other flow regimes will be investigated in a future effort.

REFERENCES

/1/ Reimann, J., John, H., Müller, U., Measurement of Two-Phase Mass Flow Rate: A Comparison of Different Techniques; to be published in Int. J. Multiphase Flow

/2/ Reimann, J., John, H., Seeger, W., Experiments on the Transition from Slug to Annular Flow in Horizontal Air-Water and Steam-Water Flow; Paper A8, European Two-Phase Flow Group Meeting, Eindhoven, The Netherlands, June 1981

/3/ Baker, O., Simultaneous Flow of Oil and Gas, The Oil and Gas Journal, p. 185, July 1954

/4/ Mandhane, J.M., Gregory, G.A., Aziz, K., A Flow Pattern Map for Gas-Liquid Flow in Horizontal Pipes, Int. J. Multiphase Flow, 1, p. 537, 1974

/5/ Taitel, Y., Dukler, A.E., A Model for Predicting Flow Regime Transitions in Horizontal and Near Horizontal Gas-Liquid Flow, A.I.Ch.E. Journal, 22, no. 1, p. 47, 1976

/6/ Simpson, H.C., Rooney, D.H., Grattan, E., A Theory for the Transition from Annular to Slug Flow in Horizontal Pipes, European Two-Phase Flow Group Meeting, University of Strathclyde, Glasgow, UK, 3rd - 6th June 1980.

/7/ Weisman, J., Duncan, D., Gibson, J., Crawford, T., Effects of Fluid Properties and Pipe Diameter on Two-Phase Flow Patterns in Horizontal Lines, Int. J. Multiphase Flow, Vol. 5, pp. 437-462, 1979.

/8/ Wallis, G.B., Vertical annular flow - a simple theory. Paper presented at AIChE Annual Meeting, Tampa, Florida, 1968

/9/ Dukler, A.E., Hubbard, M.G., A Model for Gas-Liquid Slug Flow in Horizontal and Near Horizontal Tubes, Ind. Eng. Chem. Fundam., Vol. 14, Nr. 4, pp. 337-347, 1975.

/10/ Coney, M.W.E., The Analysis of a Mechanism of Liquid Replenishment and Draining in Horizontal Two-Phase Flow, Int. J. Multiphase Flow, Vol. 1, pp. 647-669, 1974

/11/ Butterworth, D., Pulling, D.J., A Visual Study of Mechanisms in Horizontal, Annular, Air-Water Flow, AERE-M 2556, 1972

/12/ Hewitt, G.F. & Hall-Taylor, N.S. 1970 Annular Two-Phase Flow., Pergamon Press, Oxford, p. 7

/13/ Schicht, H.H., Experimentelle Untersuchungen an der adiabaten Zweiphasenströmung Wasser/Luft in einem horizontalen Rohr: Strömungsformen, Schwallströmung, Anlaufeffekte, Prom. Nr. 4547, ETH Zürich, 1970

/14/ Barnea, D., Shoham, O., Taitel, Y., Dukler, A.E., Flow Pattern Transition For Gas-Liquid Flow in Horizontal and Inclined Pipes, Comparison of Experimental Data with Theory, Int. J. Multiphase Flow, Vol. 6, pp. 217-225, 1980

/15/ Nicholson, M.K., Aziz, K.,Gregory, G.A., Intermittend Two Phase Flow: Predictive Models. 27th Can. Chem. Engng Conf., Calgary, Alberta, 1977

/16/ Govier, G.W. & Omer, M.M., The Horizontal Pipeline flow of Air-Water Mixtures. Can. J. Chem. Engng 40, 93-104, 1962

/17/ Hoogendoorn, C.J., Gas Liquid Flow in Horizontal Pipes. Chem. Engng Sci. 9, 205-217, 1959

/17/ Greskovich, E.J., Shier, A.L., Slug Frequency in Horizontal Gas-Liquid Slug Flow, Ind. Eng. Chem. Process Des. Development, Vol. 11, Nr. 2, 1972

/18/ Reimann, J., John, H., Measurements of the Phase Distribution in Horizontal Air-Water - and Steam-Water-Flow; Second CSNI Specialist Meeting on Transient Two-Phase Flow, Paris (France), 12th-14th June 1978

/20/ Kubi, J., The Presence of Slug Flow in Horizontal Two-Phase Flow, Int. J. Multiphase Flow, Vol. 5, pp. 327-339, 1979

/21/ Hewitt, G.F., Measurement of Two-Phase Flow Parameters, Academic Press, London, 1978

/22/ Müller, St., Verfahren und Einrichtung zum Identifizieren einer Zweiphasenströmung, Reaktortagung 1978, Hannover (Germany) Apr. 4-7, 1978, Deutsches Atomforum e.V., Kerntechnische Ges. im Dt. Atomforum e.V. Leopoldshafen 1978: ZAED. S. 174-177

/23/ Reimann, J., John, H., Phasenverteilung in horizontaler Luft-Wasser- sowie Dampf-Wasser-Strömung. Reaktortagung, Hannover, Apr. 4-7, 1978, Deutsches Atomforum e.V., Kerntechnische Ges. im Dt. Atomforum e.V. Leopoldshafen 1978: ZAED. S. 170-73

/24/ Reimann, J., John, H., Müller, St., Impedance Probe for Detecting Flow Regime and Measuring the Phase Distribution in Horizontal Air-Water- and Steam-Water Flow, Two-Phase Flow Instrumentation Review Group Meeting, Troy, New York, March 13-14, 1978

/25/ Reimann, J., John, H., Löffel, R., Solbrig, C.W., Chen, L.L., Goddrich, L.D., EG&G Mass Flow Rate Instrumentation Tests at Kernforschungszentrum Karlsruhe, Analyses Report Vol. 1, KfK 2812, 1979

/26/ John, H., Reimann, J., Gemeinsamer Versuchsstand zum Testen und Kalibrieren verschiedener Zweiphasen-Massenstrommeßverfahren, Anlagenbeschreibung, KfK 2731 B , Febr. 1979

/27/ John, H., Reimann, J., Alsmeyer, H., Hahn, H., Megerle, A., Serielles 5-Strahl-$\gamma$-Densitometer zur Dichtemessung einer Zweiphasenströmung, KfK 2783, Nov. 79

/28/ Simpson, H.C., Rooney, D.H., Gratton, E., and Al-Samarral, F., Two-Phase Flow in Large Diameter Horizontal Lines; Paper H6, European Two-Phase Flow Group Meeting, Grenoble, 1977

/29/ Mayinger, F., Zetzmann, K., Ähnlichkeitsuntersuchungen bei Zweiphasenströmungen: Strömungsformen bei Zweiphasenströmung in Wasser undR12, Jahresbericht IFV-GKSS, 1975.

/30/ Reimann, J., John, H., Frank, R., Measurement of Mass Flow Rate and Quality with a Venturi Nozzle and a Turbine Meter in Steam-Water Flow, Proc. OECD (NEA) CSNI Third Spec. Meet. on Trans. Two-Phase Flow, Pasadena, CA, (USA), March 1981, CSNI Report No. 61

/31/ Reimann, J., John, H., Seeger, W., Gemeinsamer Versuchsstand zum Testen und Kalibrieren verschiedener Zweiphasen-Massenstrom-Meßverfahren, KfK 2950, 1981

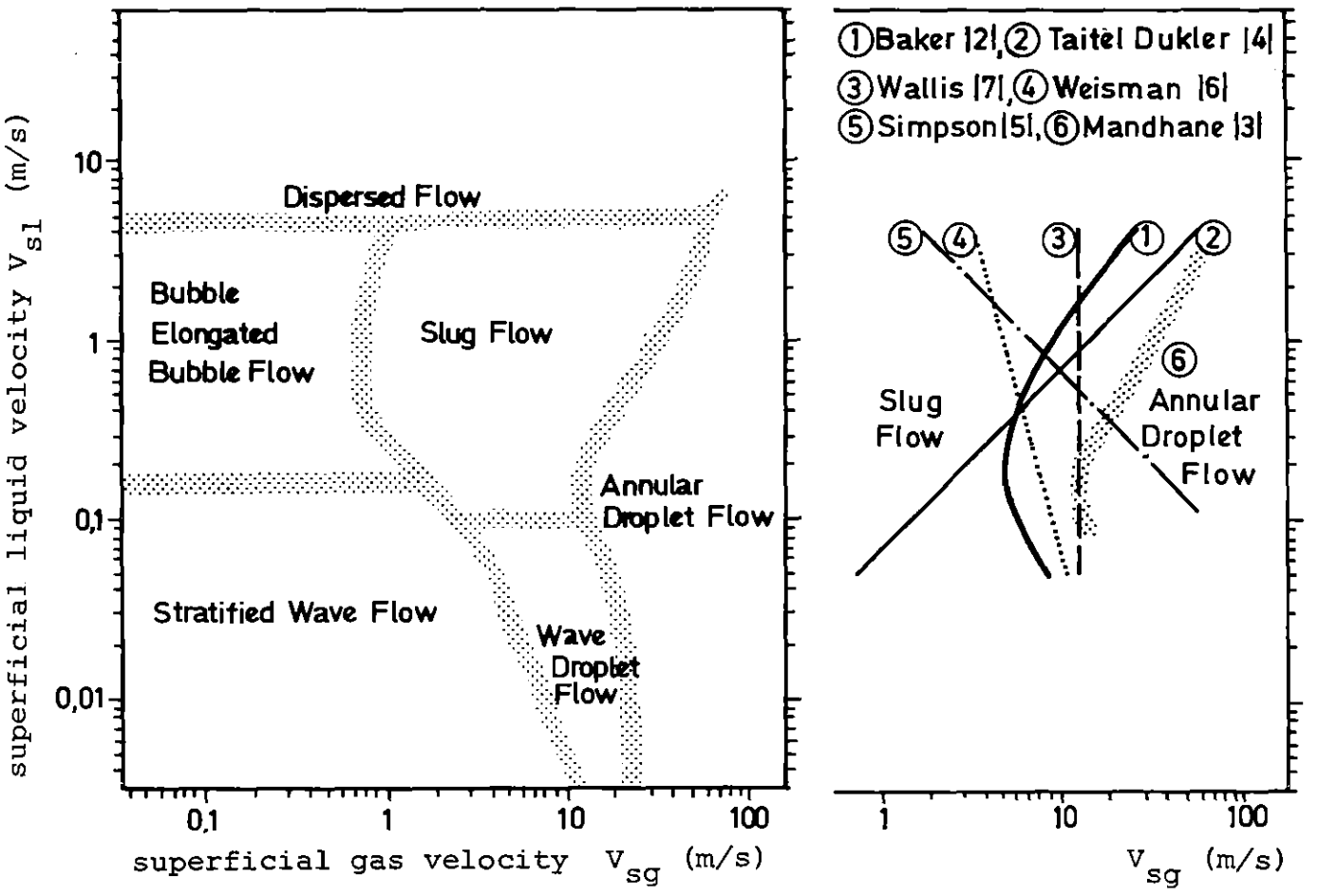


Fig. 1 Mandhane et al Flow Map (Left) and Various Correlations for the Slug-Annular Flow Regime Boundary (Air-Water Flow, $p = p_{atm}$, $d = 0,025$ m)

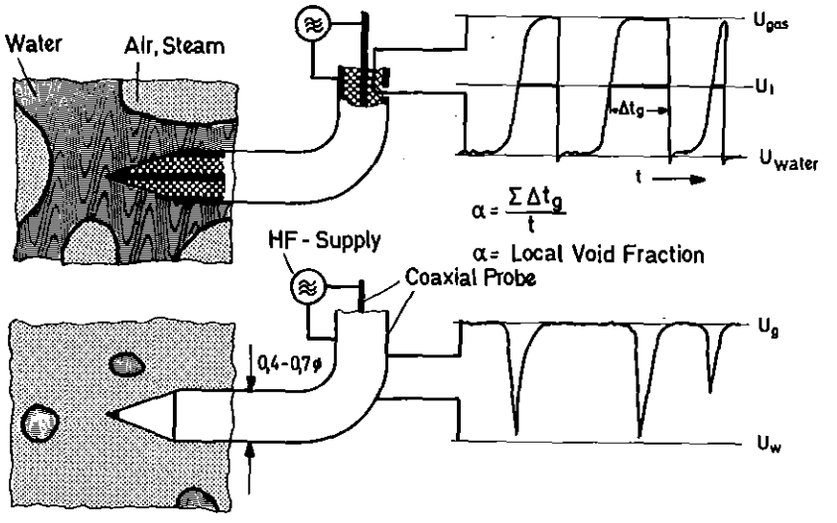


Fig. 2 Schematic Diagram of Impedance Probe

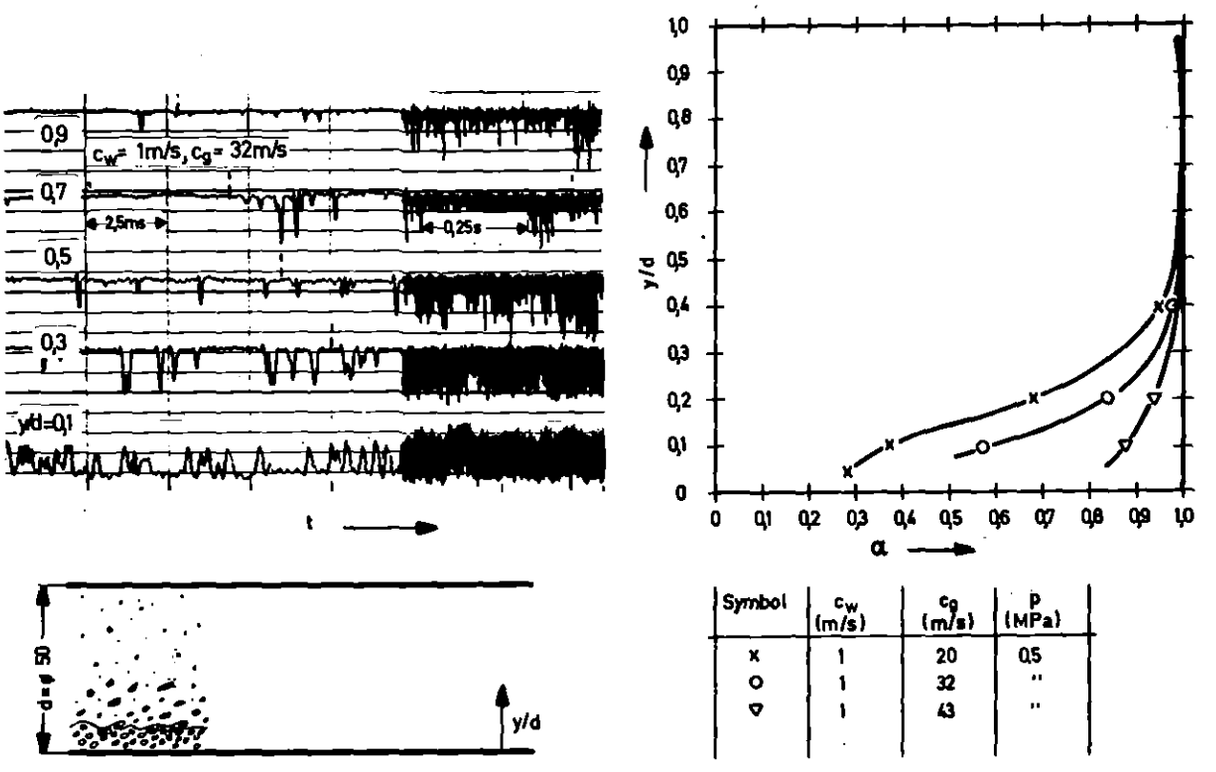


| Symbol | $c_w$ (m/s) | $c_g$ (m/s) | p (MPa) |
|---|---|---|---|
| x | 1 | 20 | 0,5 |
| o | 1 | 32 | " |
| ▽ | 1 | 43 | " |

Fig. 3 Annular Droplet Flow Pattern
(Air-Water Flow, p = 0,5 MPa, d = 0,05 m)

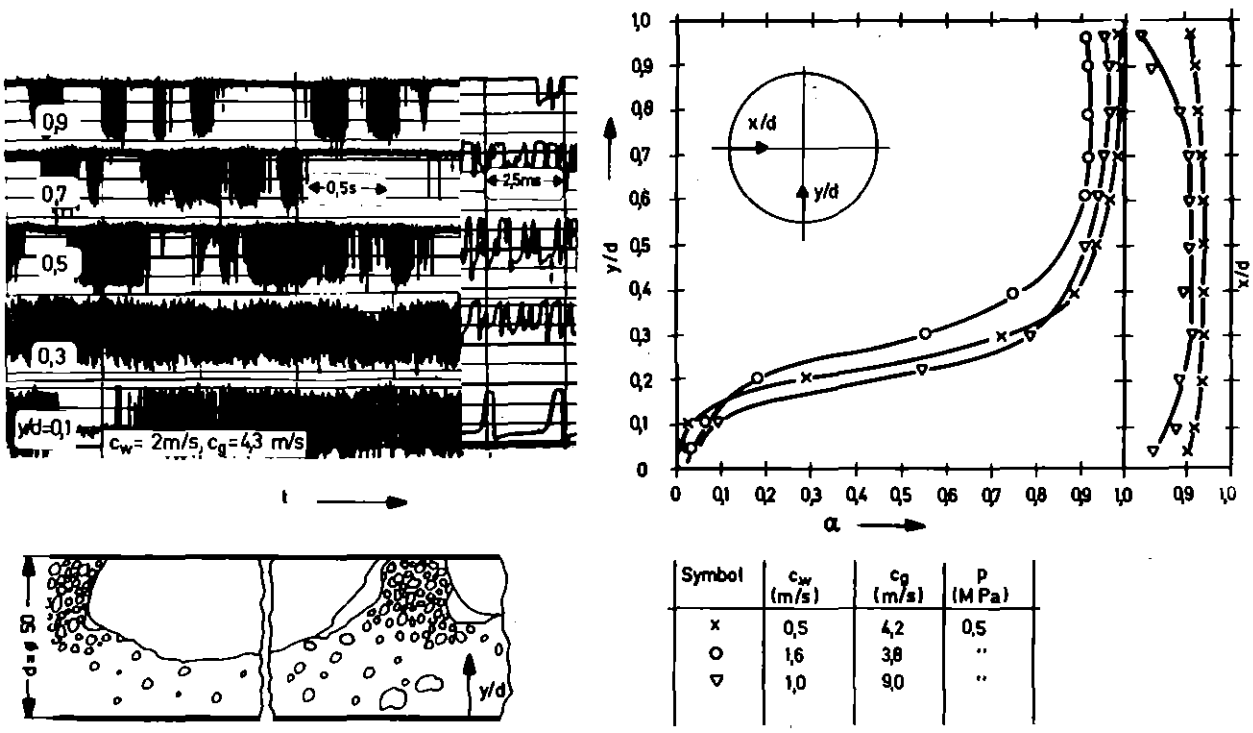


Fig. 4 Slug Flow Pattern (Air-Water Flow, p = 0,5 MPa, d = 0,05 m)

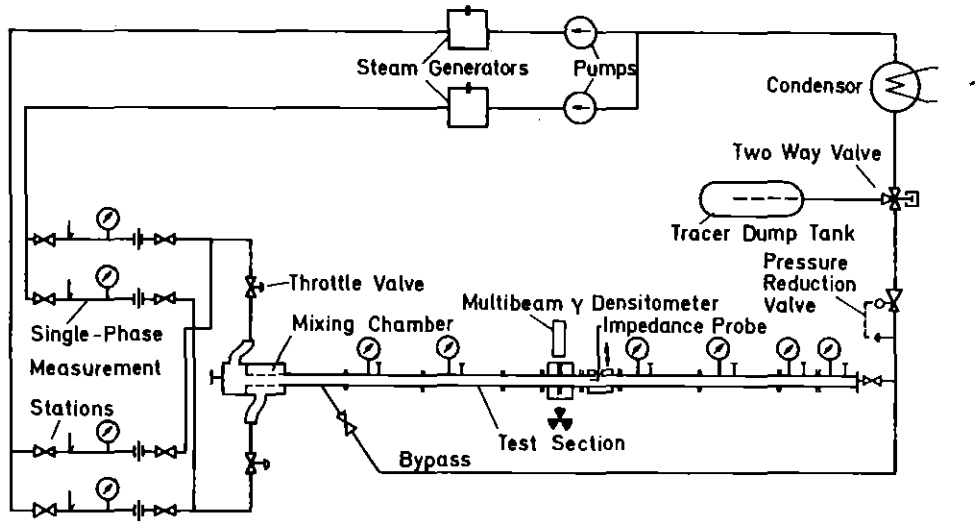


Fig. 5 Schematic Diagram of the Steam-Water Loop

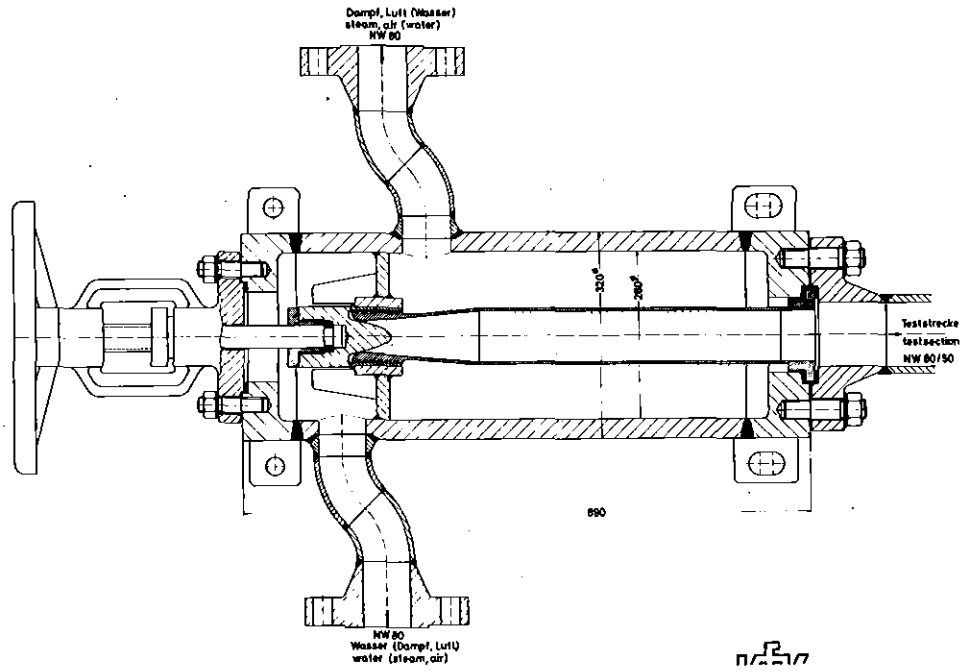


Fig. 6 Mixing Chamber

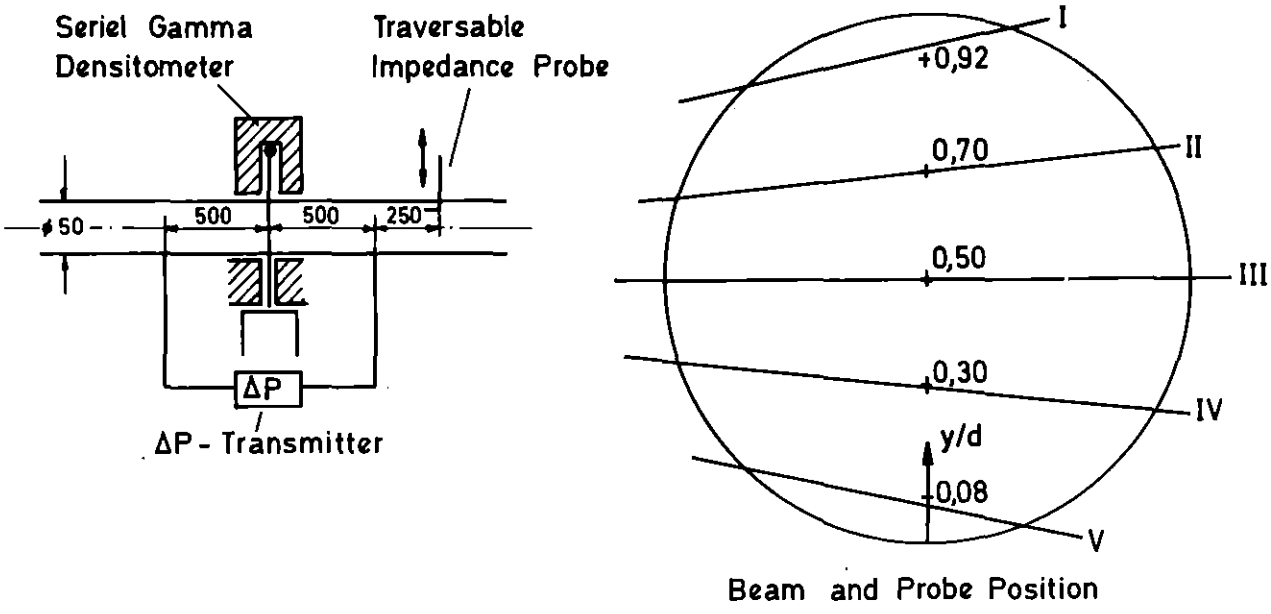


Fig. 7 Instrumentation for Flow Pattern Determination

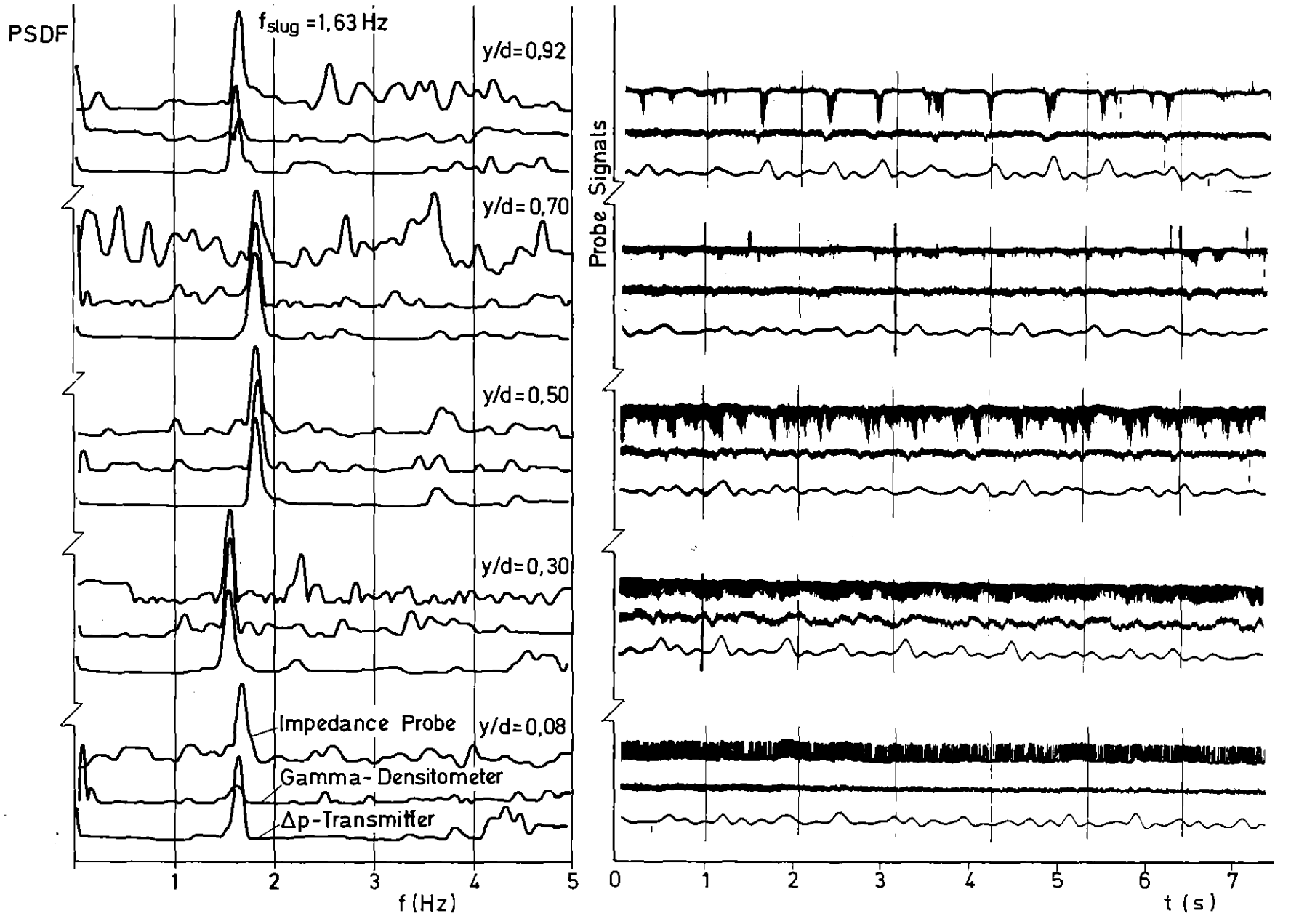


Fig. 8 PSDF and Probe Signals for Slug Flow (Steam-Water; p = 2,5 MPa; $V_{sl}$ = 1,5 m/s $V_{sg}$ = 10 m/s; d = 0,05 m)

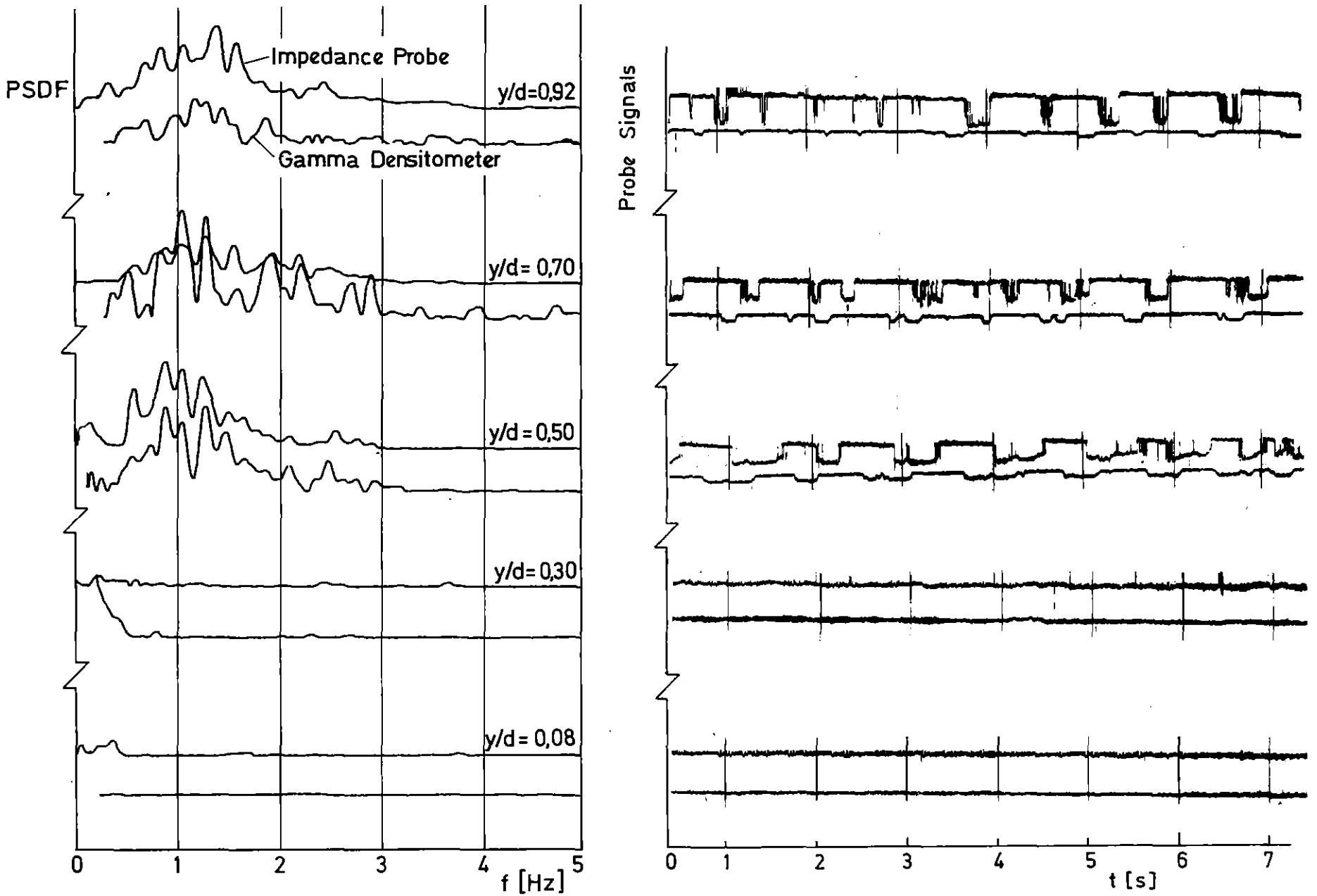


Fig. 9 PSDF and Probe Signals for Slug Flow (Steam-Water; p = 5 MPa; $V_{sl}$ = 1 m/s, $V_{sg}$ = 0,7 m/s; d = 0,05 m)

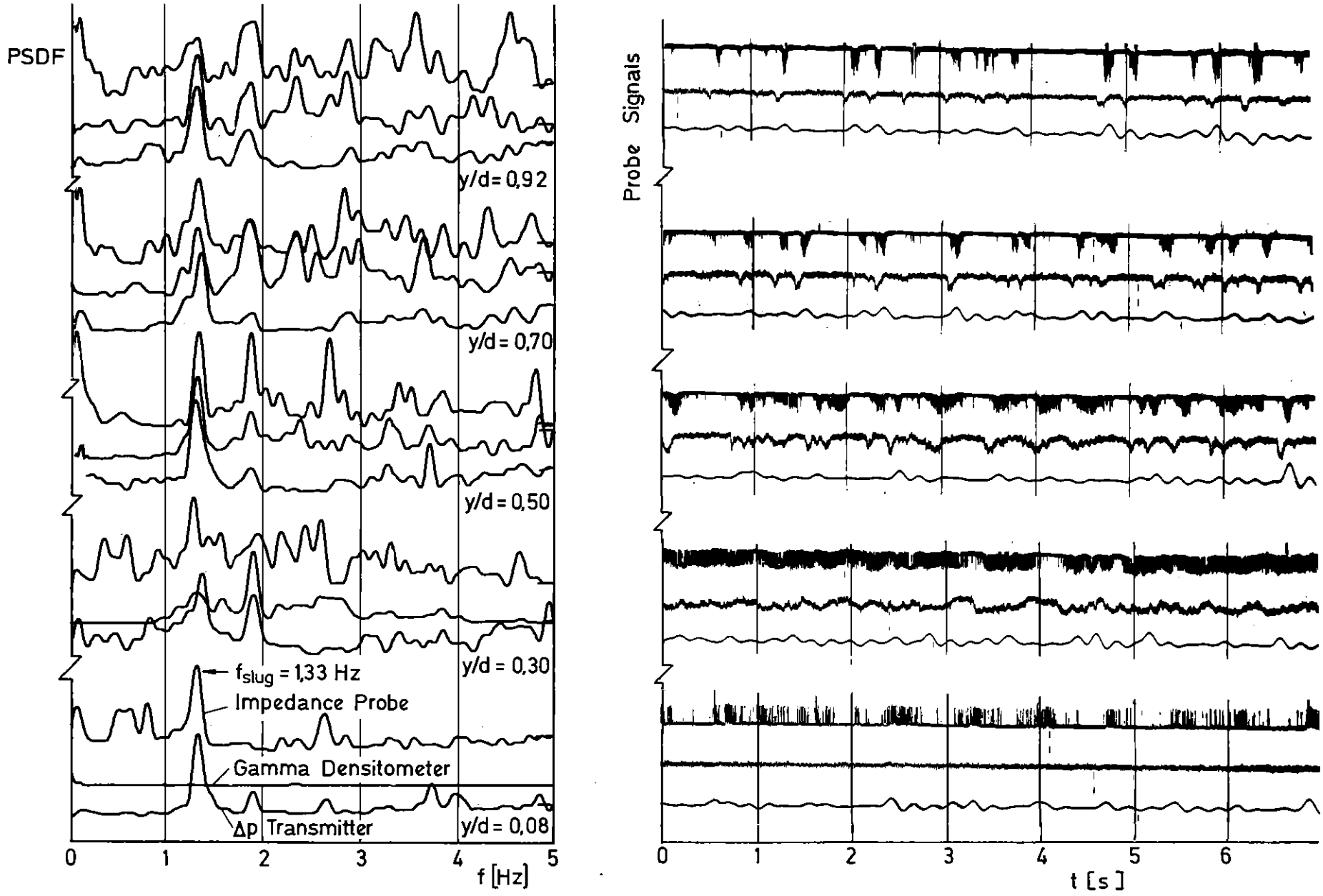


Fig. 10 PSDF and Probe Signals for Slug Flow (Steam-Water; p = 2,5 MPa, $V_{sl}$ = 1,5 m/s, $V_{sg}$ = 5 m/s; d = 0,05 m)

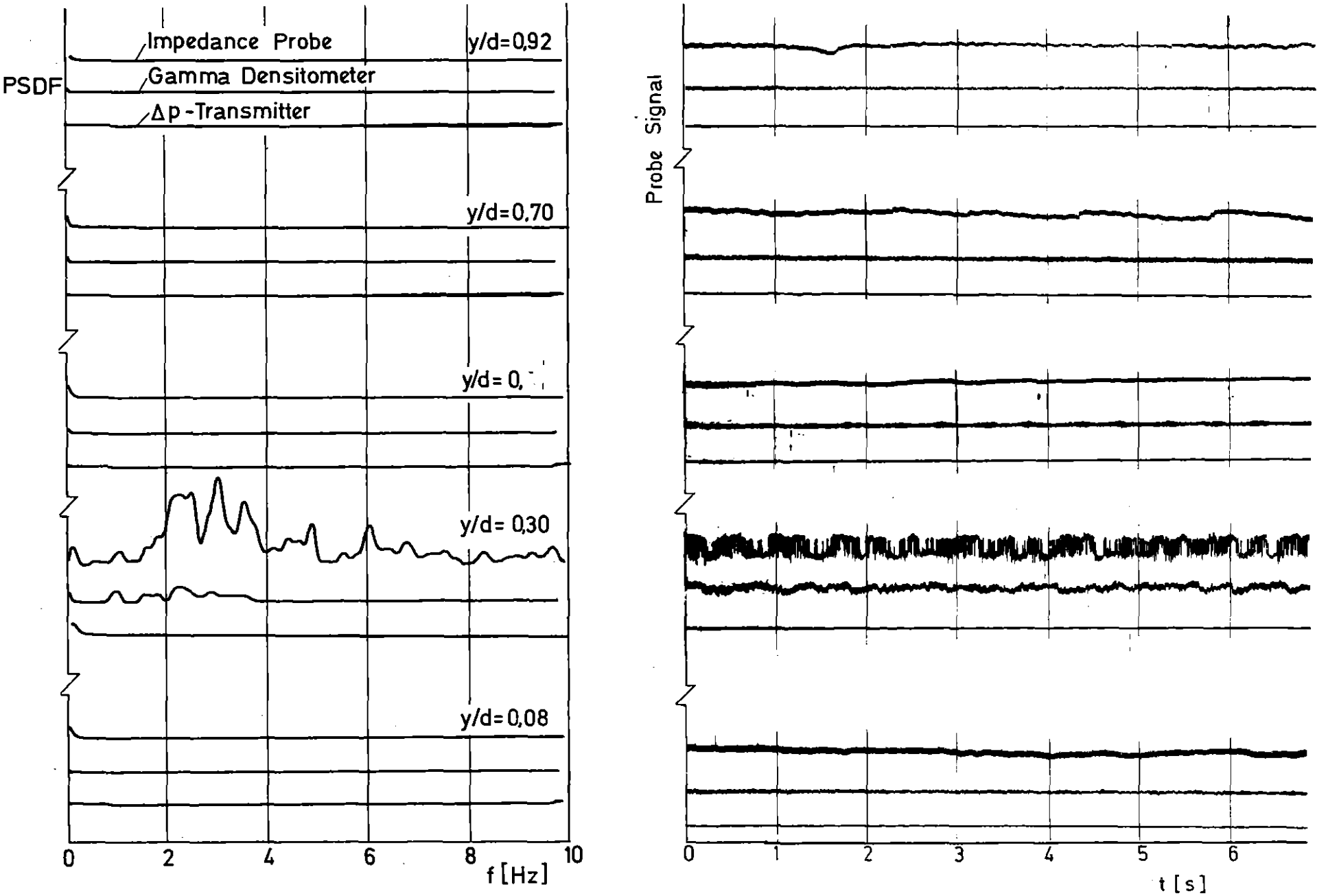


Fig. 11 PSDF and Probe Signals for Wave Flow (Steam-Water; p = 10 MPa, $V_{sl}$ = 0,27 m/s; $V_{sg}$ = 2,5 m/s; d = 0,05 m)

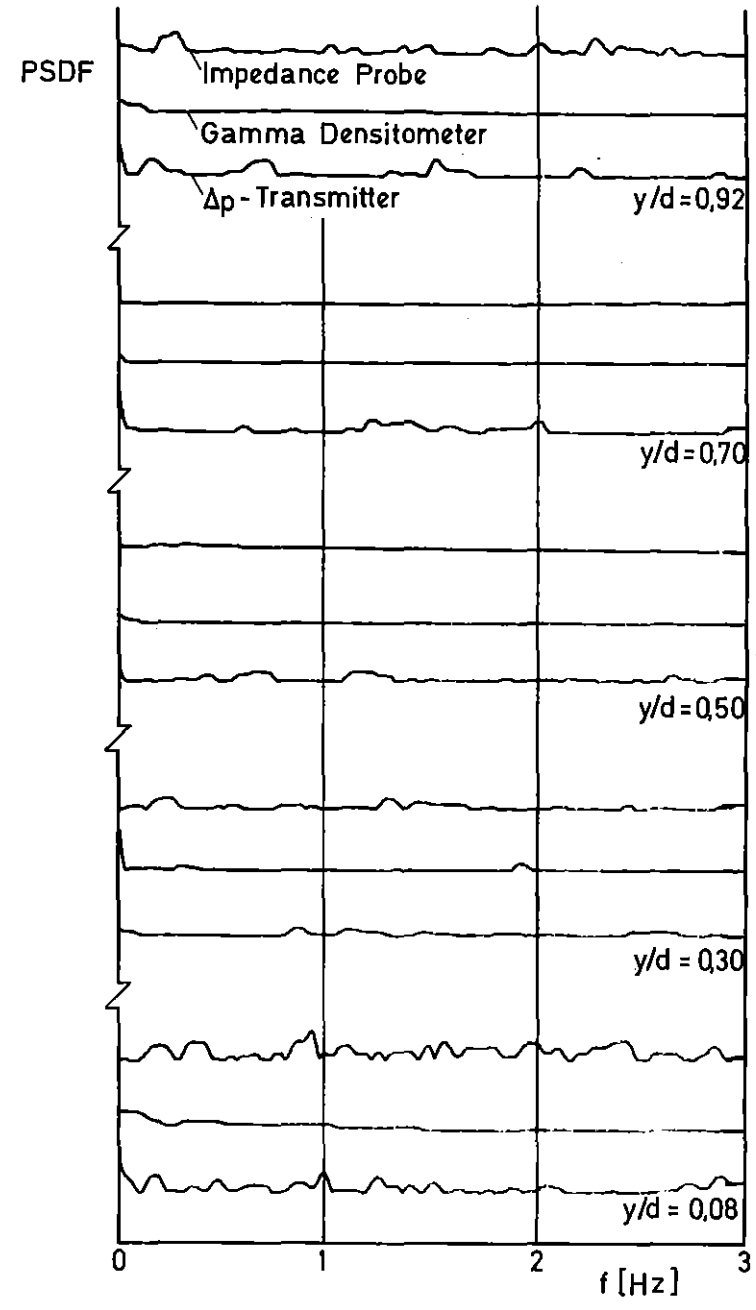


Steam - Water Flow ; p = 2.5 MPa, $V_{sl}$ = 2 m/s; $V_{sg}$ = 20 m/s ; d = 0,05 m

Fig. 12 PSDF for Annular Flow

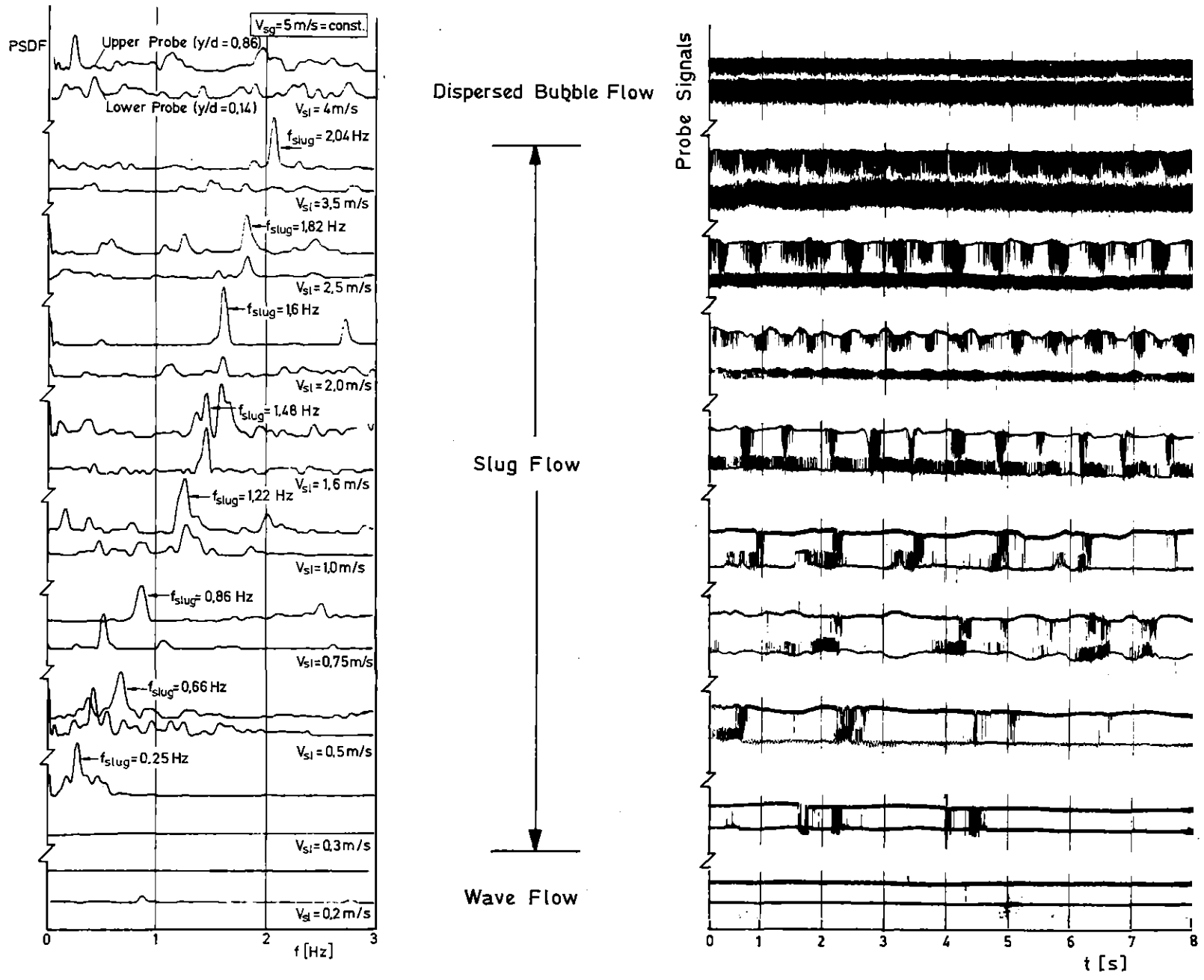


Fig. 13 PSDF and Probe Signals for $V_{sg}$ = 5 m/s (Air-Water, p = 0,5 MPa, d = 0,08 m)

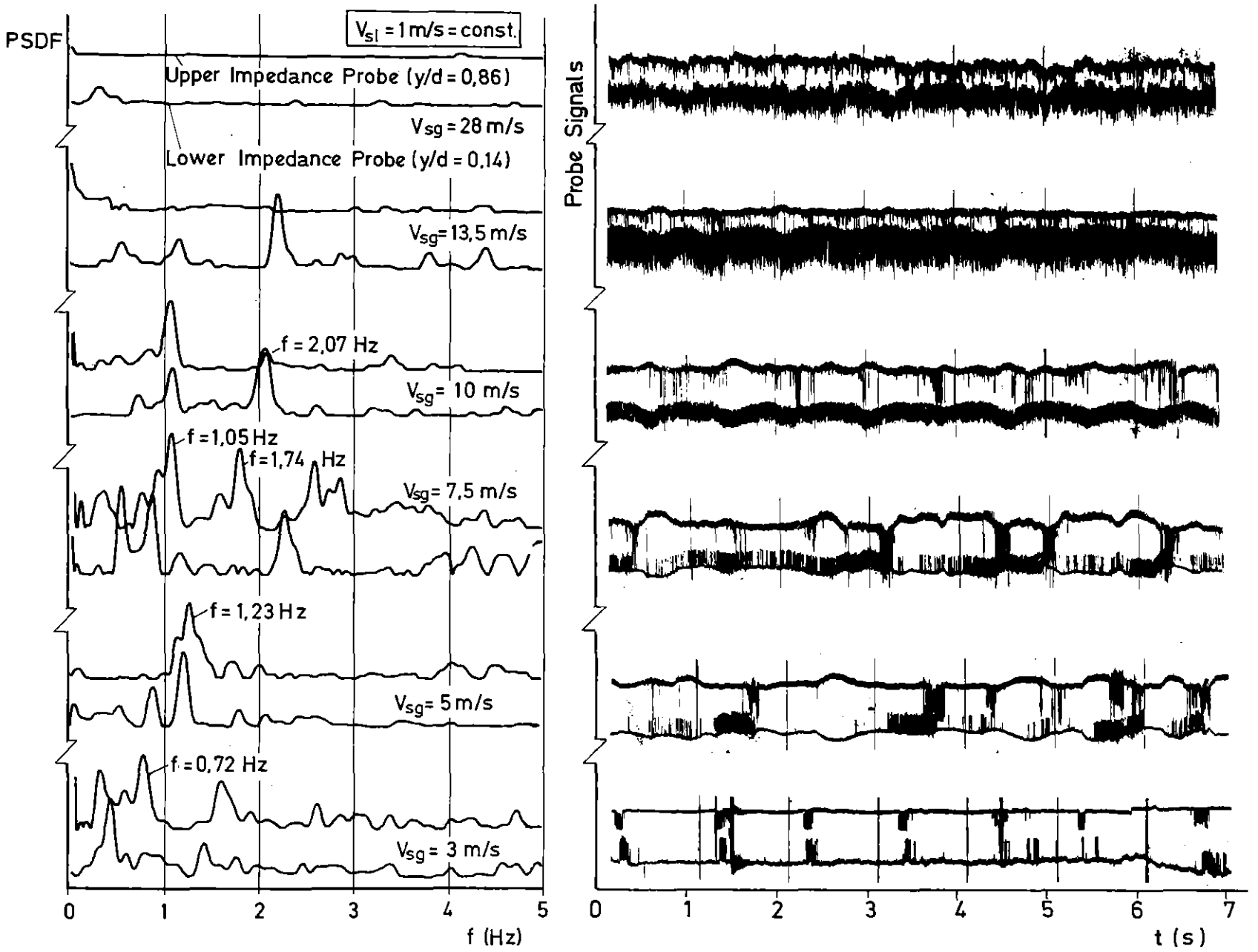


Fig. 14 PSDF and Probe Signals for $V_{sl}$ = 1 m/s (Air-Water, p = 0,5 MPa; d = 0,08 m)

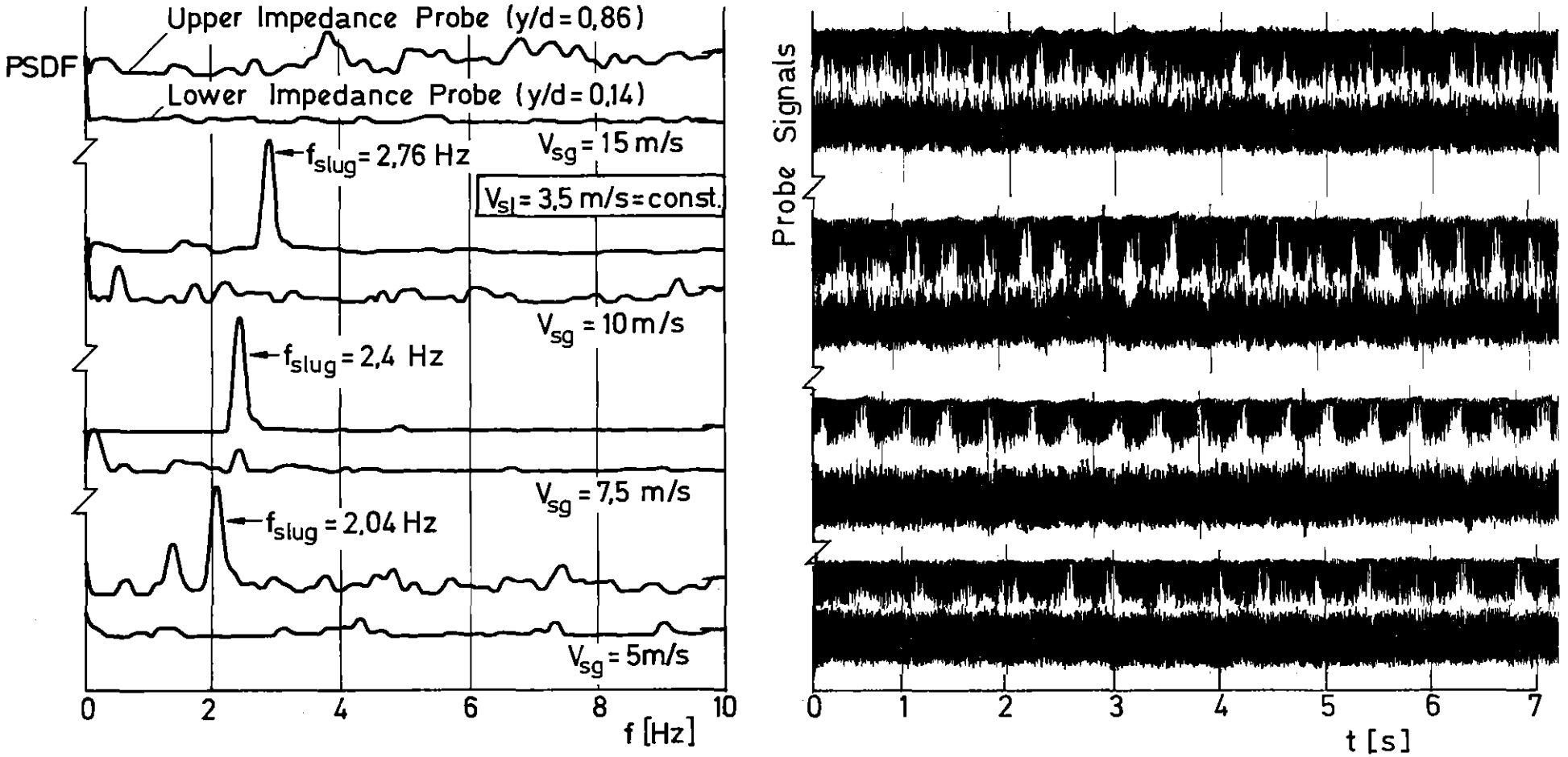


Fig. 15 PSDF and Probe Signals for $V_{sl}$ = 3,5 m/s (Air-Water, p = 0,5 MPa; d = 0,08 m)

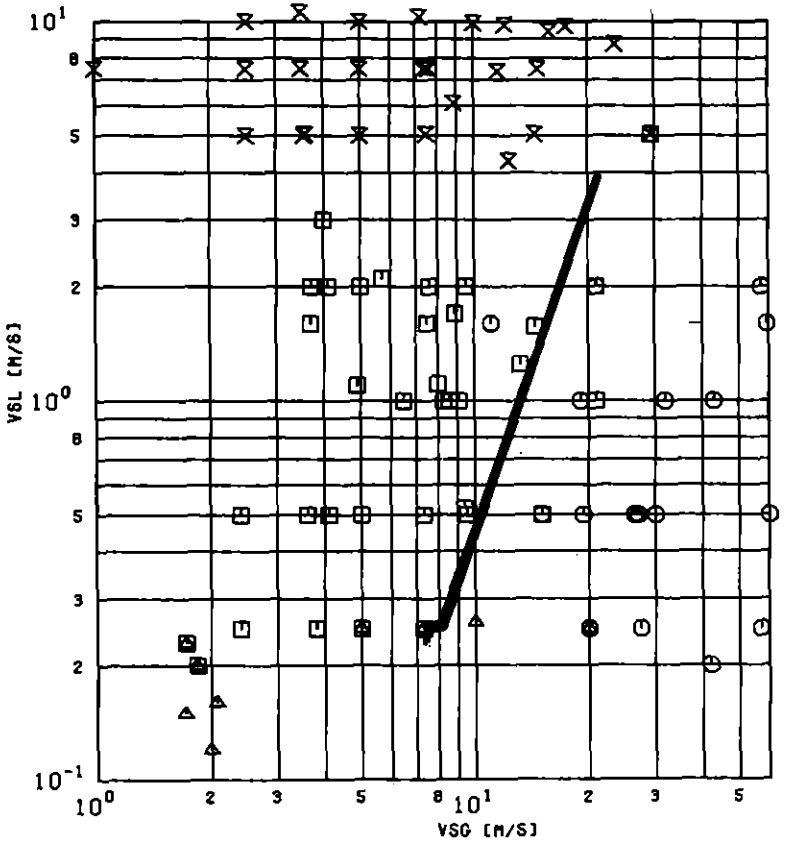


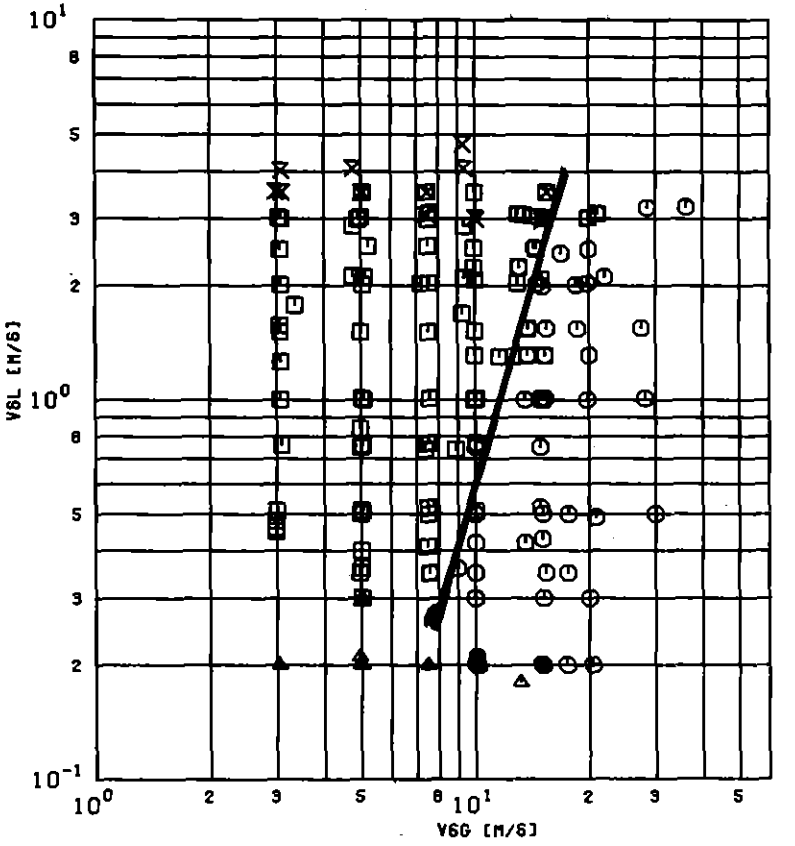


□ slug; ○ annular; ✕ dispersed; △ wave
▣ slug-annular; ▨ slug-wave
⊠ slug-dispersed; ◭ wave-annular

Fig. 16 Flow Pattern: Air-Water Flow
p = 0,5 MPa, d = 0,05m

Fig. 17 Flow Pattern: Air-Water Flow
p = 0,5 MPa; d = 0,08 m

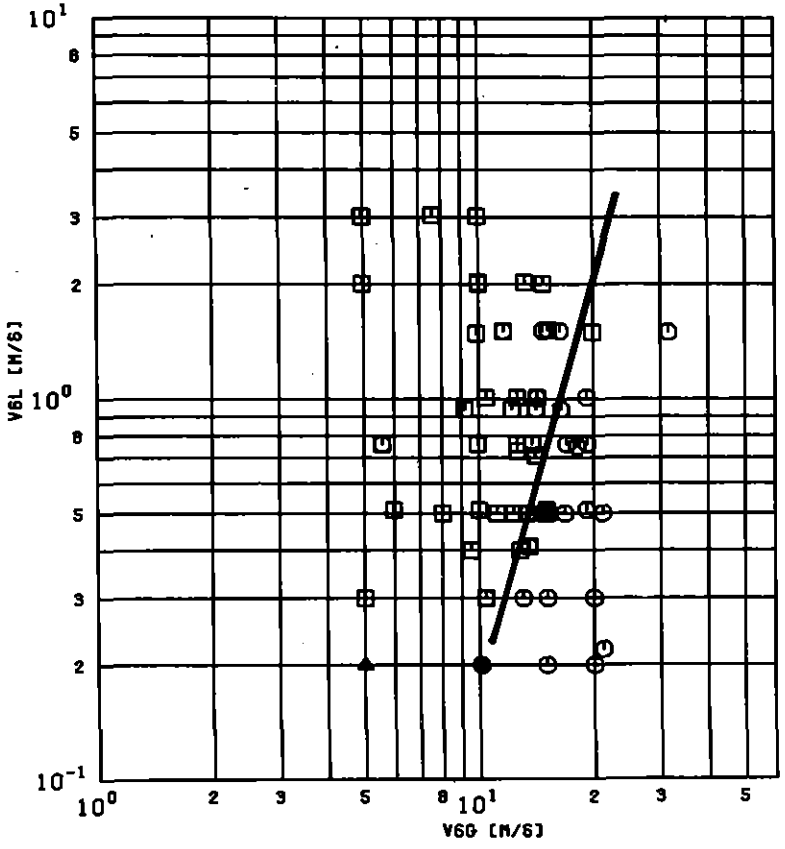


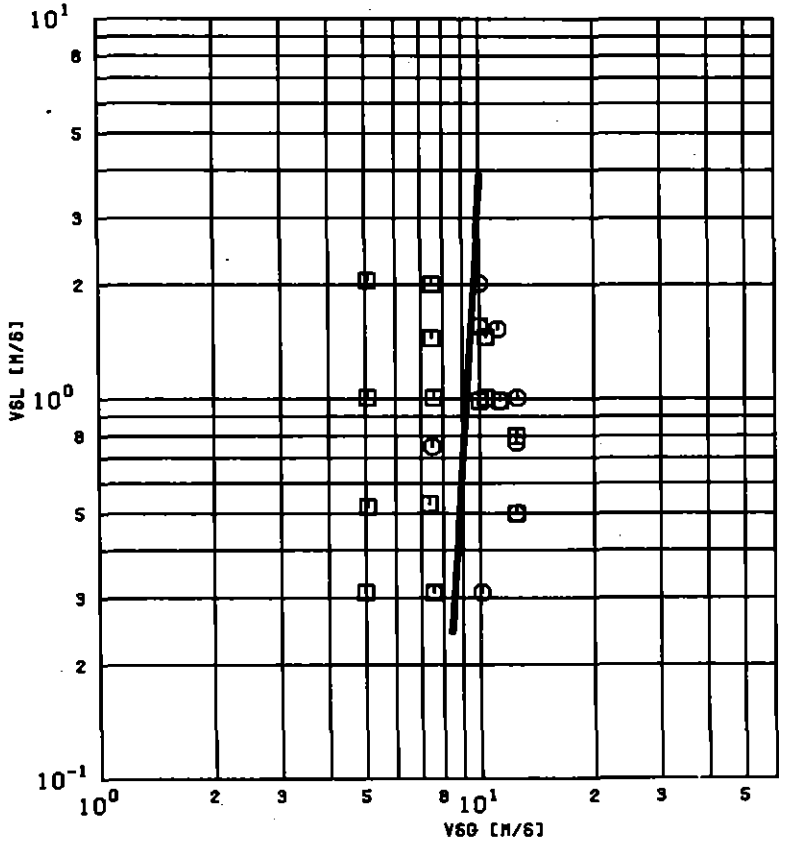


□ slug; ○ annular; X dispersed; △ wave
◘ slug-annular; ◬ slug-wave
⊠ slug-dispersed; ◭ wave-annular

Fig. 18 Flow Pattern: Air-Water Flow
p = 0,2 MP; d = 0,08 m

Fig. 19 Flow Pattern: Air-Water Flow
p = 0,5 MPa; d = 0,08 m
Mixing Chamber Revolved by 180°

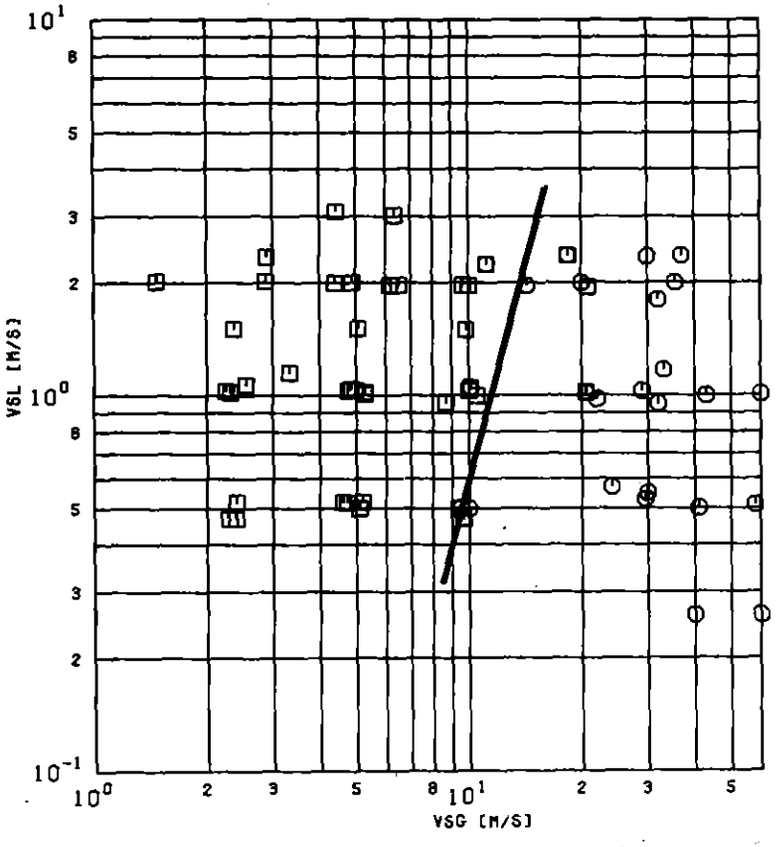


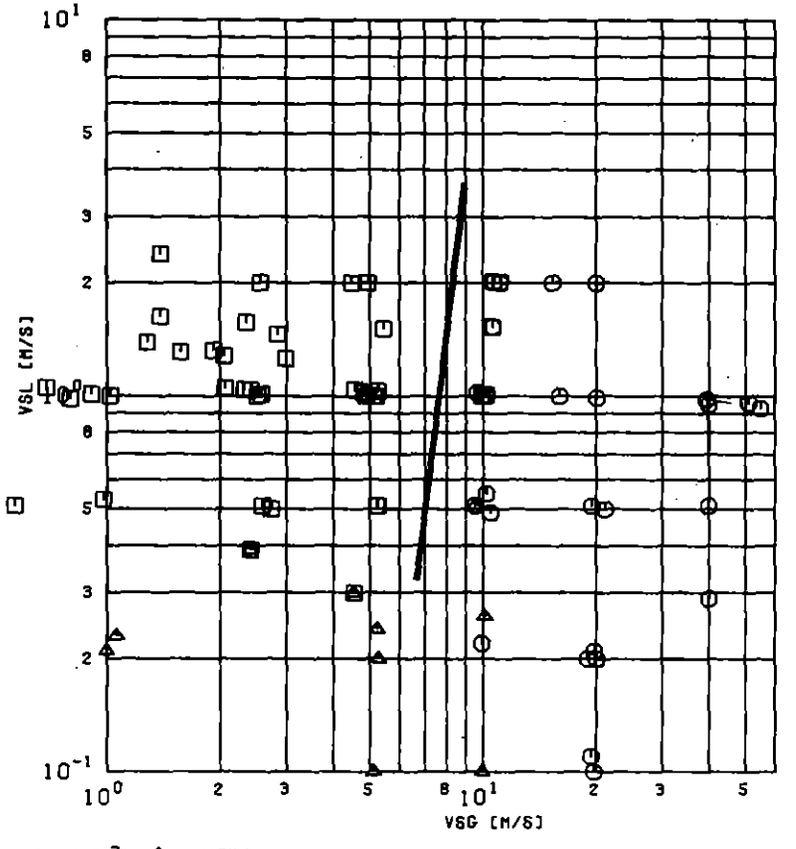


□ slug; ○ annular; X dispersed; △ wave
◘ slug-annular; ⧋ slug-wave
⊠ slug-dispersed; ⧊ wave-annular

Fig. 20 Flow Pattern: Steam-Water Flow
p = 2.5 MPa; d = 0,05 m

Fig. 21 Flow Pattern: Steam-Water Flow
p = 4 MPa, 5 MPa; d = 0,05 m, 0,066 m

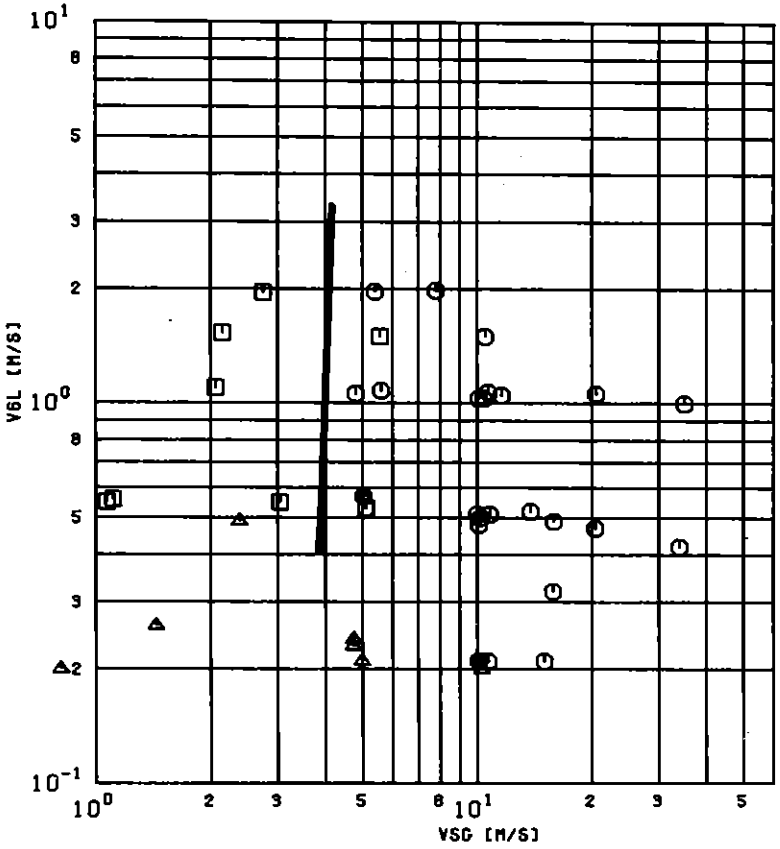


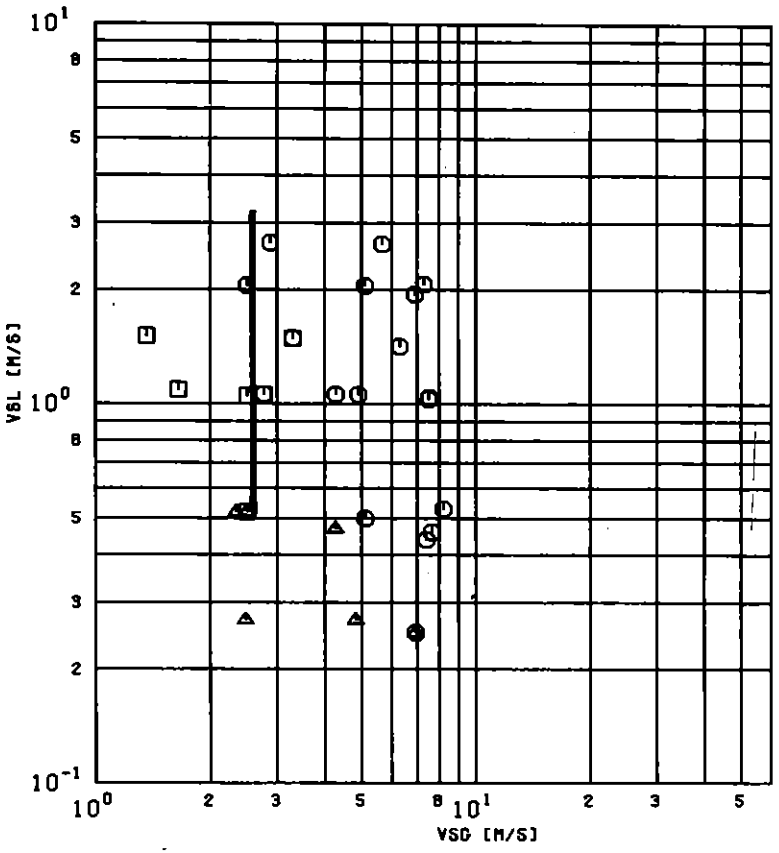


□ slug; ○ annular; ✕ dispersed; △ wave
◘ slug-annular; ⧈ slug-wave
⊠ slug-dispersed; ◬ wave-annular

Fig. 22 Flow Pattern: Steam-Water Flow
p = 7,5 MPa; d = 0,05 m, 0,066 m

Fig. 23 Flow Pattern: Steam-Water Flow
p = 10 MPa; d = 0,05 m

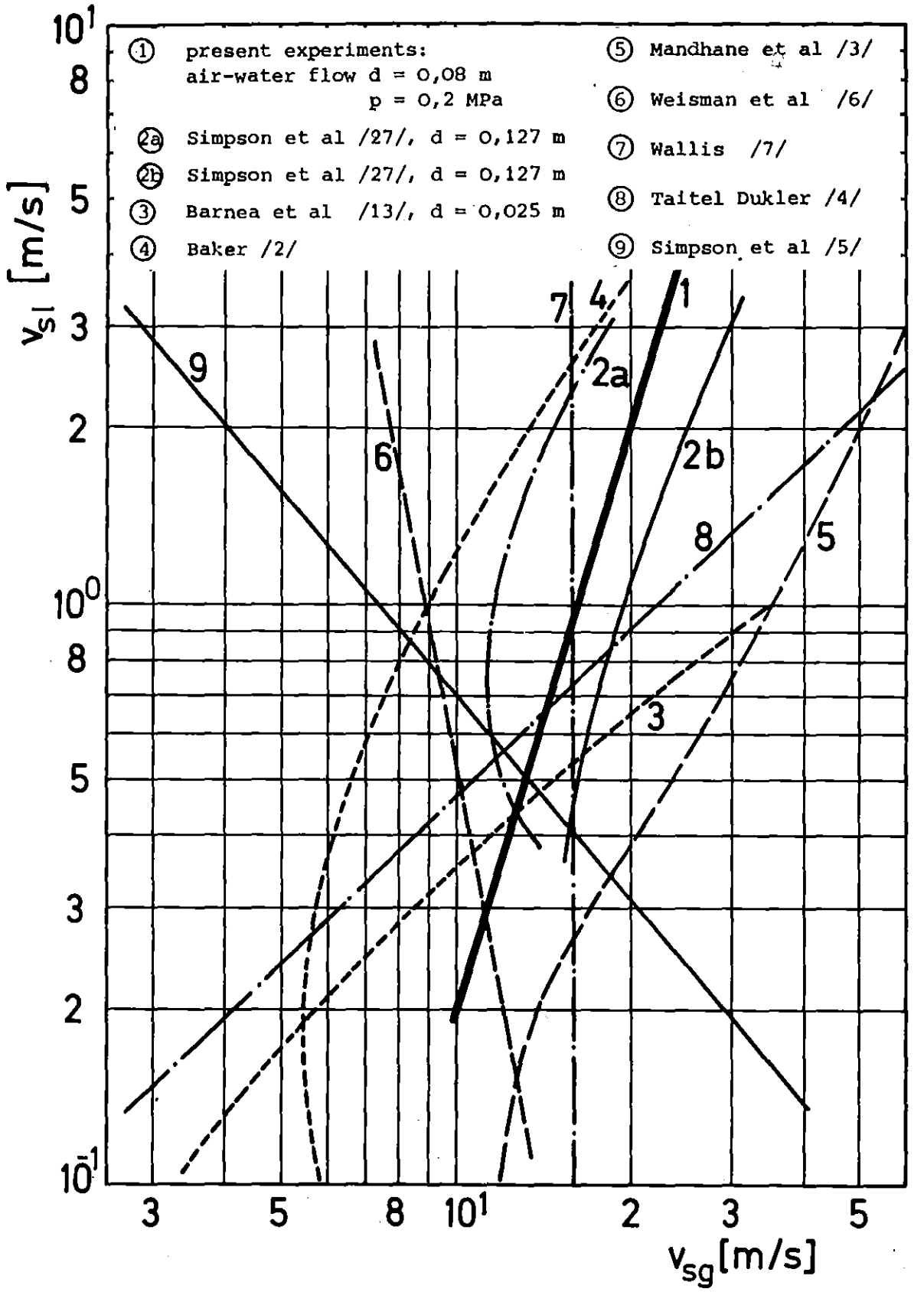


Fig. 24 Slug-Annular Flow Boundary
(d = 0,08 m, Air-Water Flow at p = 0,2 MPa)

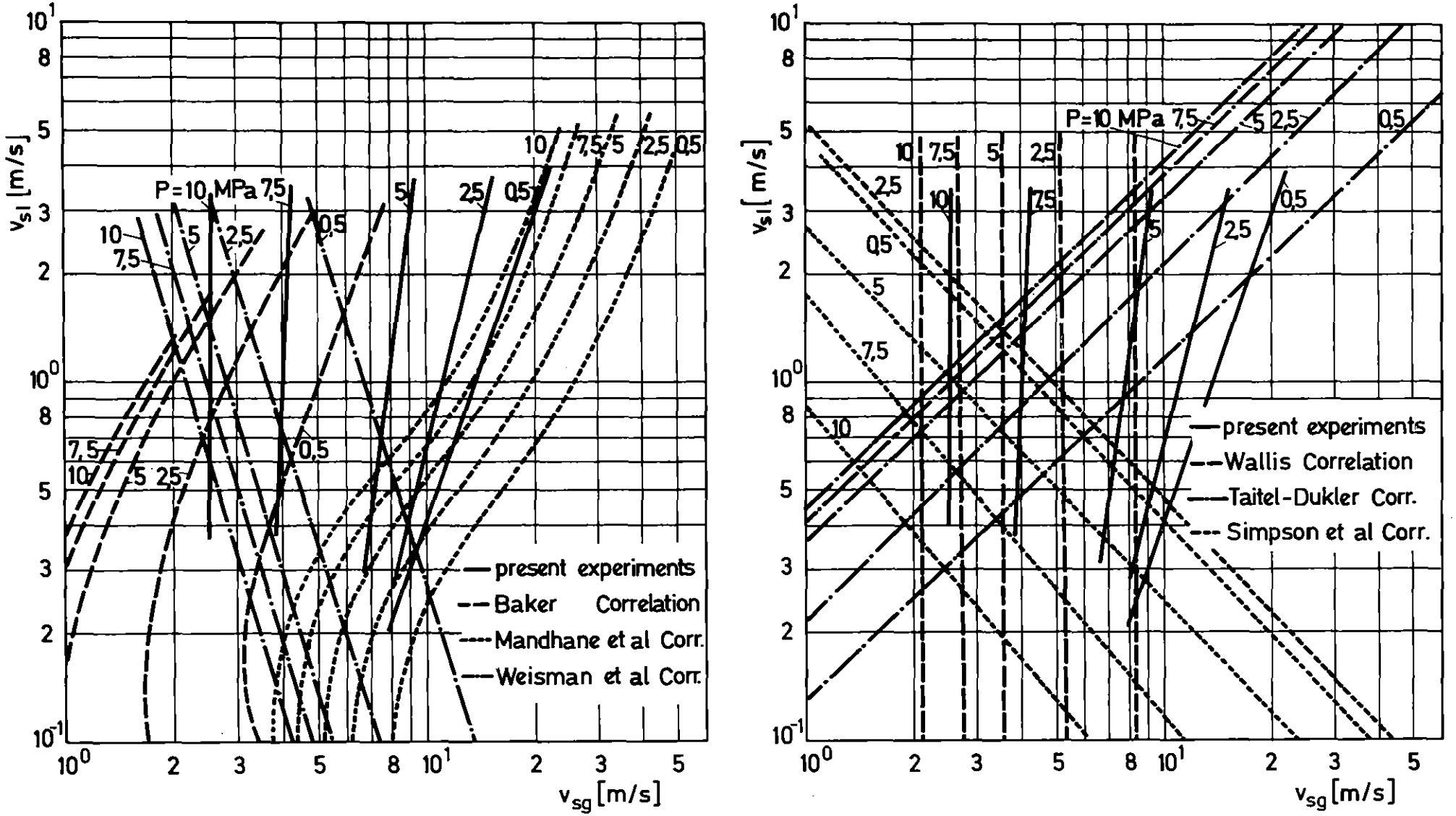


Fig. 25 Slug-Annular Boundary
(d = 0,05 m; Air-Water Flow at p = 0,5 MPa, Steam-Water Flow at p = 2,5 - 10 MPa)

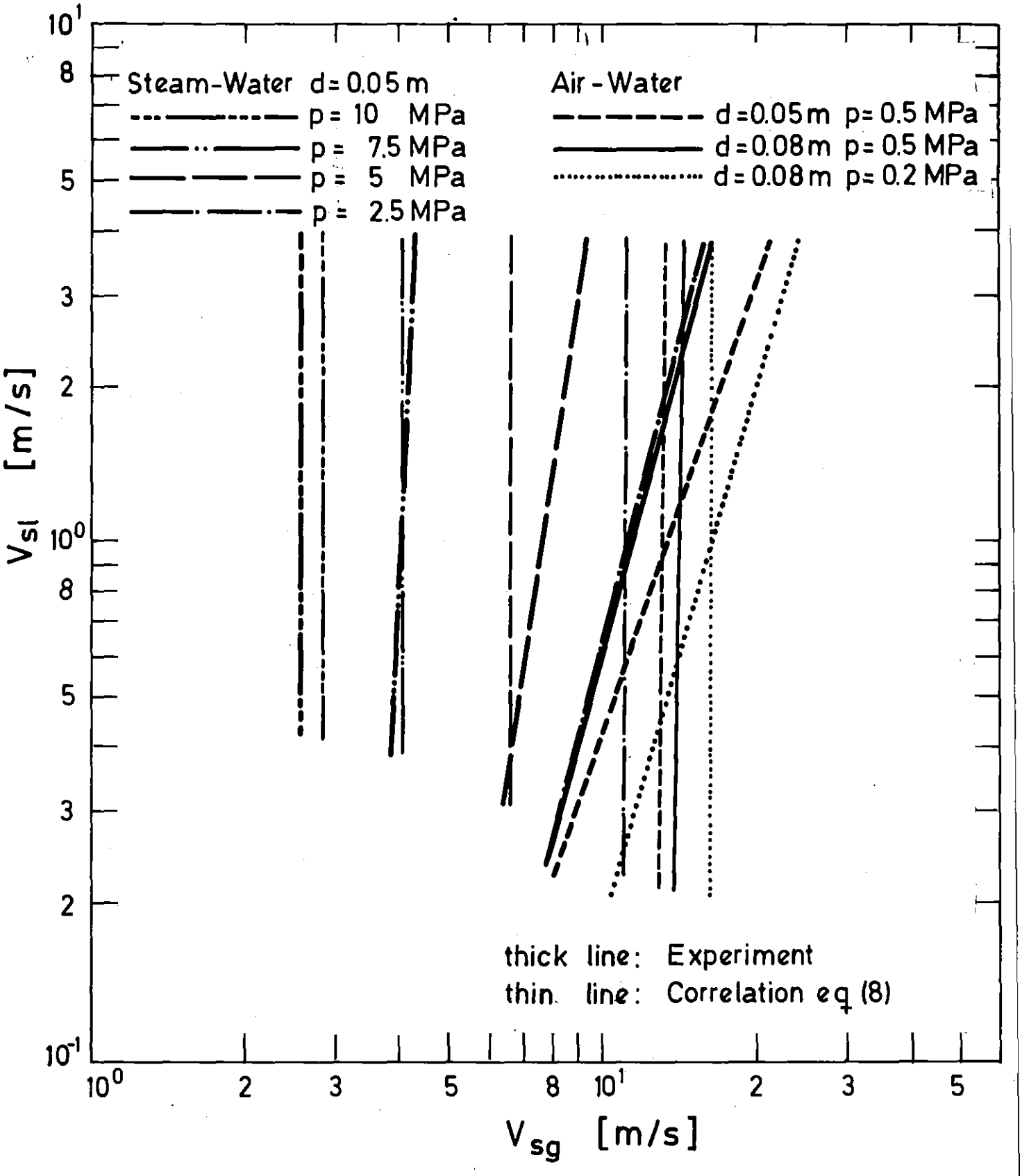


Fig. 26 Comparison between Experimental Data and New Correlation